Effect of Temperature and Strain rate on Flow behavior of $Al_{0.3}CoCrFeNi$ HEA

PALLEDA THAVITI NAIDU

A Dissertation Submitted to

Indian Institute of Technology Hyderabad

In Partial Fulfillment of the Requirements for

The Degree of Master of Technology

भारतीय प्रौद्योगिकी संस्थान हैदराबाद
Indian Institute of Technology Hyderabad

Department of Materials Science and Metallurgical Engineering

June, 2019

Declaration

I declare that this thesis submission illustrates my own thoughts in my own words, and also others' concepts or words have been comprised, I have adequately cited and referenced the original sources. I also announce that I have adhered to all principles of academic honesty and integrity and have not misrepresented or falsified any idea/data/fact/source in my submission. I know that any violation of the above will be a reason to take disciplinary action by the Institute and can also evoke penal action from the sources that I have not been cited properly, or from whom proper consent has not been taken when needed.
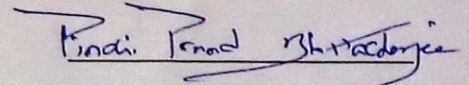
P. Thaviti naidu

_____

(Signature)

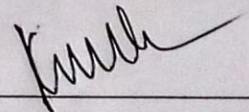PALLEDA THAVITI NAIDU

(MS17MTECH11008)

Approval Sheet

This thesis entitled "**Effect of temperature and strain rate on flow behavior of Al$_{0.3}$CoCrFeNi HEA**" by **Palleda Thaviti Naidu** is approved for the degree of Master of Technology from IIT Hyderabad.

Dr. Pinaki P.Bhattacharjee

Department of Materials Science and Metallurgical Engineering
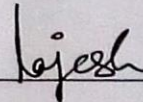
Examiner

Dr. Sairam K Malladi

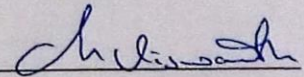Department of Materials Science and Metallurgical Engineering

Examiner

Dr. Rajesh Korla

Department of Materials Science and Metallurgical Engineering

Advisor

Dr. Chinthapenta R Viswanath

Department of Mechanical and Aerospace Engineering

Chairman

Acknowledgement

Abstract

High-entropy alloys (HEAs) are currently attracting much interest because they offer unique properties and good ductility at low temperatures. These materials are of interest primarily because they contain five or more principal elements, with each element having a concentration between 5 and 35 at. %, and yet they have very simple structures based on solid solution phases.

Super plasticity is major concern for forming industries to fabricate complex and curves components, to use in automotive, aerospace and other application. In addition to that, the materials used in automobile and other structural applications often encountered with shock loadings. Recent experiments have shown that the HEAs also have a potential for exhibiting superplastic property when testing at elevated temperatures. Since super-plasticity requires a very small grain size, typically < 10 μm, it is feasible to introduce significant grain refinement by thermomechanical processing.

The main aim of this work is to develop $Al_{0.3}CoCrFeNi$ high entropy alloy with very fine equi-axed stable grain microstructure using proper thermomechanical treatment. Study the deformation behavior both at room and high temperature. Explore the possibility of super plasticity. Further, study the effect of temperature and strain rate on the deformation behavior.

keywords: High Entropy alloy, Microstructure, High temperature tensile, Super plasticity Fractography

Nomenclature

HEA	:	High Entropy Alloy
ECAP	:	Equal-Channel Angular Pressing
HPT	:	High-Pressure Torsion
ICP-MS	:	Inductively Coupled Plasma Mass Spectrometry
EDM	:	Electro-Discharge Machine
DIC	:	Digital Image Correlation
SEM	:	Scanning Electron Microscopy
EBSD	:	Based Electron Backscattered Diffraction
EDS	:	Energy-dispersive X-ray spectroscopy
At%	:	Atomic Percentage
VHN	:	Vickers Hardness Number
RC	:	Recrystallized
RD	:	Rolling Direction
TD	:	Transverse Direction
GBS	:	Grain Boundary Sliding
UTS	:	Ultimate Tensile Stress

Contents

List of Figures

List of Tables

Chapter 1: Introduction

1.1 Overview:

The conventional alloy design strategies based on one principle alloying element with one or more minor alloying additions, enhances mechanical properties, compared to pure metals, through different strengthening mechanisms like, solid solution strengthening, precipitation hardening. Based on the number of major alloying components, they are classified as binary, ternary, quaternary and so on. Alloys can form solid solution depends on the mutual solubility of components which can be determined by Hume –Rothery rules, namely; - atomic size difference, relative valance, crystal structure and electronegativity. Limited solubility results in the formation of terminal solid solutions. Except Isomorphous alloy systems, most of the fundamental metallurgical theories and principles demonstrates that multiple alloying elements favors the formation of intermetallic compounds which are brittle in nature. These brittle Intermetallic phases deteriorates the mechanical properties and make them difficult to processing and thereby limits their application as a structural material. Further conventional alloying approach, limits the number of alloys that can be studied and utilized.

High Entropy Alloy(HEA) design is the recent development consists of blend of 5 or more elements with each element concentrations between 5 and 35 atom percentage [1], [2]. Studies showed that, due to high entropy of mixing, high entropy alloys can form simple BCC, FCC or mixed solid solution structures with superior mechanical properties [2]. Further, this new alloy design approach allows to investigate vast, unexplored arena of alloy compositions thereby have very high potential to produce superior alloys.

There are four core effects used to describe high entropy alloy: (1) severe lattice distortion, (2) high-entropy effect, (3) sluggish diffusion effect, and (4) cocktail effect. [1] The first three are hypotheses and the cock-tail effect is unique character of High entropy alloy. The four core effects are suggested based on interpretation from the literature available. [3]

HEAs exhibits interesting physical and mechanical properties such as, excellent resistance to wear and corrosion resistance [4][5][6], good creep resistance [7][8] and fatigue resistance [9] and low thermal conductivity [10] [11]. HEA systems like Al_xCoCrFeNi with low stacking fault energy (SFE) have higher tendency for twinning leads to strain hardening results high strength with excellent formability [12] [13] In addition, due to sluggish long-range diffusion, diffusion-related processes, including crystallization, grain growth, and phase transformations are expected to be slow which leads to good thermal stability.

So far the research on mechanical behavior of high entropy alloys mainly focused micro-hardness and plastic deformation of HEAs at quasi-static strain rate region under temperatures ranging from cryogenic to room temperatures [24-28]. Unfortunately, at room temperature most of the HEAs have low ductility limits the formability. Formability, especially superplastic flow gives an extra advantage for forming industries to components with complex shapes, especially in automotive, aerospace and other application. Most of the literature suggest that fine stable equi-axial grain size is the microstructural prerequisite along with high strain rate sensitivity, resistance to cavitation to achieve superplastic flow [29]. Grain refinement is the best method to get fine grain sized structure. Exceptional grain refinement can be possible by Severe plastic deformation(SPD) which involves techniques like equal-channel angular pressing (ECAP) or high-pressure torsion(HPT). And fine-grain structure can also be achieved by thermo-mechanical processing which involves cold rolling with subsequent annealing. Presence of second phase at the grain boundaries and triple junctions help to stabilize the fine grain size during deformation at high temperature which is essential for superplastic deformation. So, choosing an alloy composition which can produce a microstructure with fine grain size and stable second phase at the grain boundaries may exhibits super plasticity at high temperature.

Present work is focusing on tensile deformation behavior of thermo-mechanically processed $Al_{0.3}$CoCrFeNi HEA consists of FCC phase with dispersion of B2 precipitates at grain boundaries. Room temperature deformation behavior was studied with the help of tensile experiments at quasi static strain rate ($1 \times 10^{-3} s^{-1}$). Further, possibility of super plasticity was explored by conducting high temperature experiments at different strain rates ($10^{-4} s^{-1}$ -$10^{-1} s^{-1}$).

Chapter 2: Literature Study

2.1 Background:

High entropy alloys (HEAs) are new class of alloys, they are quite different from traditional alloys in terms of alloy design. These alloys consist of multi-principal elements taken in equiatomic or near equiatomic ratio with or without minor alloying additions [1]. These alloys named as High entropy alloys because of their high configuration entropy due to presence of more number of elements results in the formation of simple structure solid solutions rather forming intermetallic with complex crystal structure [2]. Configuration entropy, ΔSmix can be calculated using Boltzmann's hypothesis with following expression.

$$\Delta S_{\text{mix}} = -\text{R} \sum_{i=1}^{n} X_i \ln X_i \quad \text{...................Eq (1)}$$

where R is the gas constant, 8.314 J/K mol, X_i is mole fraction and n is the number of the elements.

2.1.1 Four Effects:

Four 'core effects' are often used to describe HEAs: the high entropy effect; the lattice distortion effect; sluggish diffusion; and the 'cocktail' effect. Three of these are hypotheses and the 'cocktail' effect is a separate characterization of HEAs. These hypotheses were proposed based on earlier studies reported in the literature [3].

2.1.2 The high entropy effect:

The high entropy effect is the most important concept in HEAs and proposes that amplified configurational entropy in alloys with five or more principle elements may favors the formation of random solid solutions rather than compounds. Due to enhanced mutual solubility between the constituent elements, the number of phases present in the alloy system reduces.

As the Gibbs free energy of mixing, ΔG_{mix}, is

$$\Delta G_{\text{mix}} = \Delta H_{\text{mix}} - T\Delta S_{\text{mix}} \quad \text{................. Eq (2)}$$

Where ΔG_{mix} is Free energy of mixing (J mol^{-1}), ΔH_{mix} is Enthalpy of mixing (J mol^{-1}), ΔS_{mix} Entropy of mixing (J K^{-1} mol^{-1}),T is absolute Temperature(K).

It is clear from the above expression that with increasing the entropy of mixing, it is possible to lower the free energy and thereby made the phase more stable. In conventional alloys, solid solutions have higher entropy of mixing than IM phases. Due to the multi-principle elementals, in high entropy alloys(HEAs), the configurational entropy of solid solution is much large than intermetallic compounds and hence the free energy of solid solution phase can be much lower compared to intermetallic phases. Thus, a solid solution phases are more stable even at higher temperatures than ordered intermetallic phases. The overall order in high entropy alloys (HEAs) reduces with increasing temperature. Hence an alloy that contains ordered phases at lower temperatures will transform to solid solutions at elevated temperatures.

The XRD pattern in figure 2.1 shows the influence of high entropy effect in formation of solid solutions with simple crystal structures [14] and it is clear that all alloys systems from quinary to septenary forms simple FCC and BCC structures due to high entropy effect. [14].
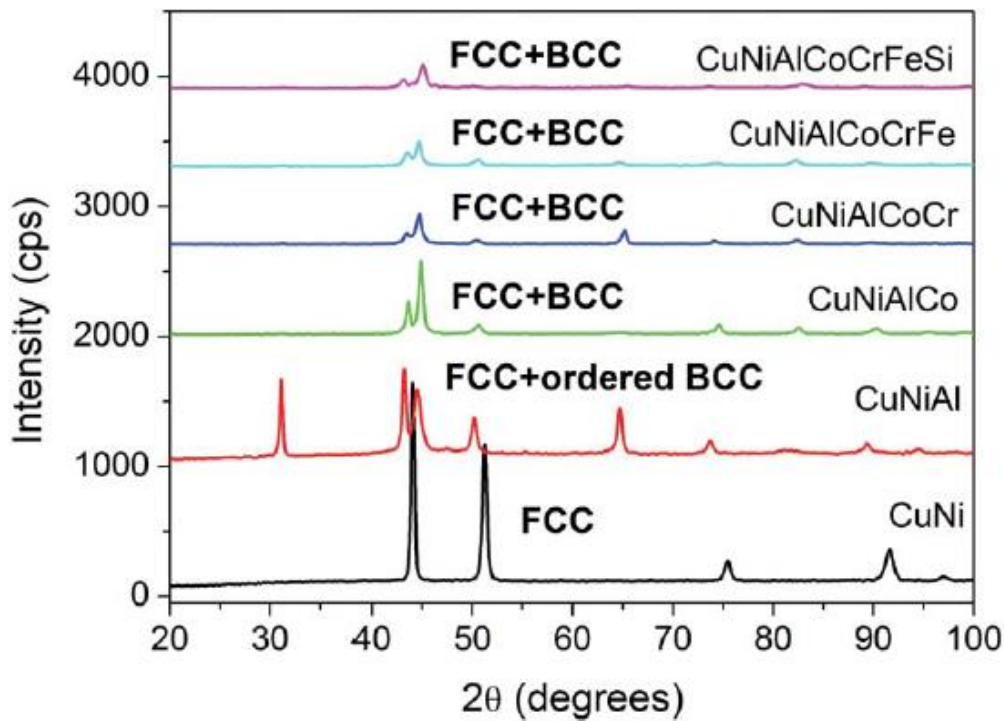
Figure 2.1 XRD pattern of alloy designed with sequential addition of new element [14].

2.1.3 Severe lattice distortion effect:

In HEAs the crystal lattice is occupied by atoms with different atomic sizes. This differences in atomic size introduces severe lattice distortion in HEAs compared to the conventional alloys where the matrix atoms usually surround the same kind of atoms as shown in figure 2.2. The sever lattice distortions increases the strength of the alloy in the form of solution hardening [14]. Lattice distortion would affect not only the mechanical properties but also reduce the thermal and electrical properties effectively due to electron and phonon scattering [15]. Severe lattice distortion also increases the free energy of the system due to strain energy and they will lead to phase transformations. As an example, Figure 2.3 illustrating the phase transformation in $Al_xCoCrFeNi$ HEA with increase in Al content. [14] [16] [17].
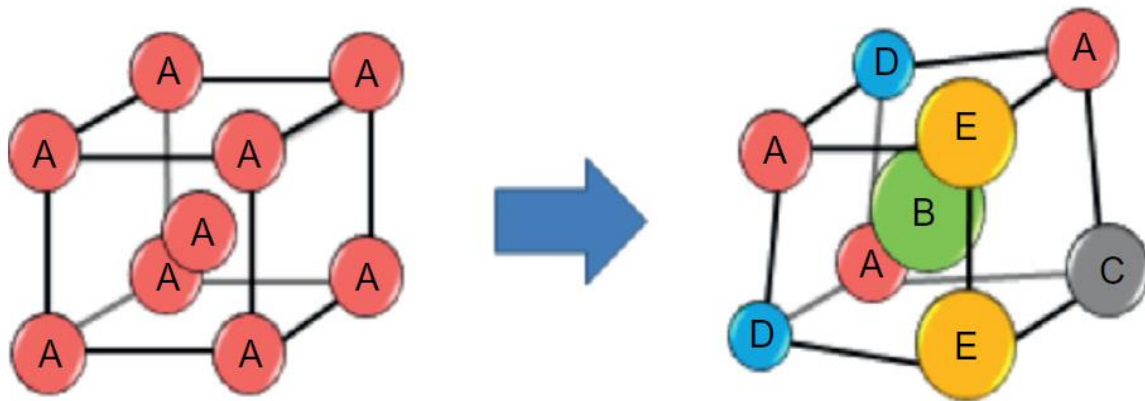
Figure 2.2 Schematics of (a) perfect lattice with similar atoms (b) severe lattice distortion of different elements [15]
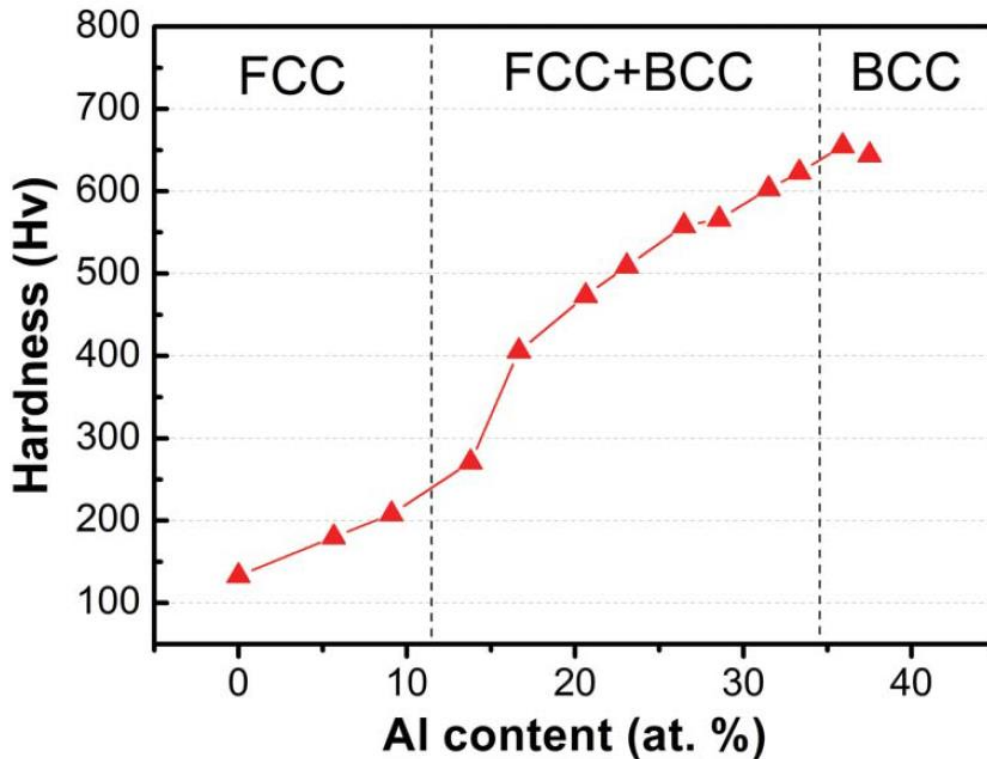
Figure 2.3 Hardness of the AlxCoCrFeNi alloys as a function of Al content [14] [16] [17]

2.1.4 Sluggish diffusion effect:

Phase transformations depend on atomic diffusion different elements with different atomic radii to attain the equilibrium partitioning. However, the vacancy diffusion of substitutional elements is limited in the high entropy alloys as compared to the conventional alloys because, a vacancy in the matrix is surrounded and competed by different components during the diffusion. Since every element has the same possibility of occupying the vacancy, it would impede the vacancy movement and end up decreasing the effective diffusion rate. In addition, large fluctuation of lattice potential energy between lattice sites because of presence of different substitutional elements which further, trap and hinder the atomic flow and lead to the sluggish diffusion effect. Therefore, it is believed that high entropy alloys would exhibit slower diffusion rates and higher activation energy compared to pure metals and traditional alloys, such as stainless steels. As shown in Figure 2.4, the elements in HEA system displays the lowest diffusion coefficients compared to other alloy systems. Due to the sluggish diffusion effect,

HEAs are capable of reaching a supersaturated state, higher recrystallization temperature, slower grain growth, and higher creep resistance, which can be helpful when it comes to controlling microstructure and mechanical properties. Moreover, it is proposed that the sluggish diffusion of HEAs would not only to produce extraordinary high temperature strength and structure stability, but also helps in the formation of nano precipitates because the nuclei are easier to generate but would difficult to grow. [18] [19] [20] [21].
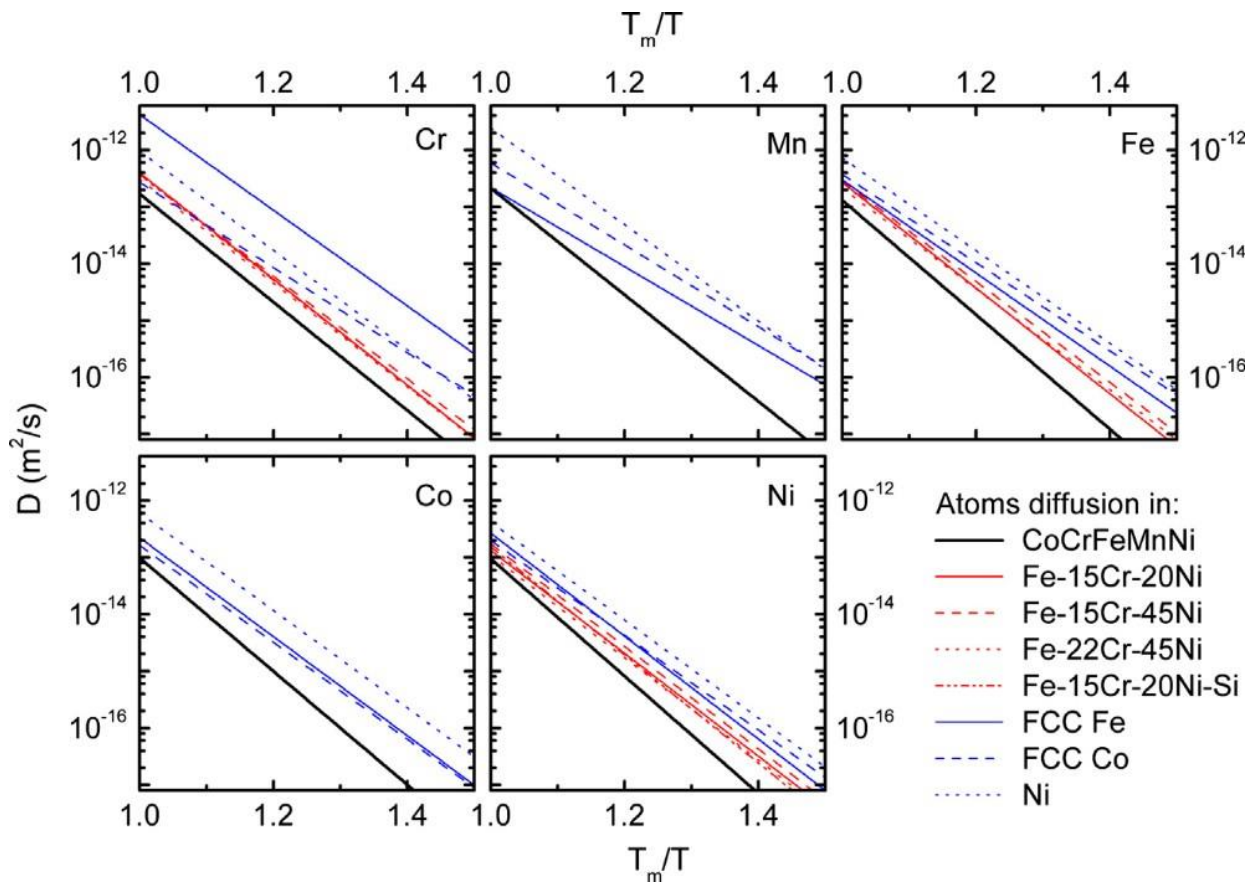
Figure 2.4 Temperature dependence of the diffusion coefficients of Co, Cr, Fe, Mn and Ni in different alloys [18].

2.1.5 Cocktail effect:

Ranganathan [22]. Suggested that HEAs are synergistic mixtures where the end result is unpredictable and greater than the sum of the individual elements. Since there are at least five

different principle elements in HEAs, they can be viewed as atomic- scale composites. So the macroscopic properties of HEAs not only depends on the individual elements but also depends on the mutual interaction between different atoms, and the lattice distortion, microstructure. One of the several examples are shown in Figure 2.3, where the hardness of the high entropy alloy can be changed considerably by adjusting the Al content in the AlxCoCrFeNi HEAs [23].

2.2 Literature review:

High entropy alloys have superior properties such as good corrosion-resistance, high thermal stability, low thermal conductivity, along with excellent mechanical properties such as excellent wear resistance, formability, very good creep and fatigue resistance [3]. Early studies on mechanical properties of HEAs focused on micro-hardness and compression date. There is a rapid increase in number of publications on HEAs in the past decade and studies relevant to the present work is summarized below.

Shun and Du *et.al*., [24] studied the microstructure and tensile behavior of FCC $Al_{0.3}CoCrFeNi$ high entropy alloy in as cast, aged at 973K (700˚C) and aged at 1173K (900˚C) conditions and observed L_{12} ordered spherical nano precipitates in as-cast condition and platelet morphology in sample aged at 973K (700˚C). Stress strain curve showed the yield drop and low strain hardening rate suggesting that the nano precipitates observed in the matrix are coherent GP zones and dislocations cutting through the precipitates as the prime strengthening mechanism. Alloy aged at 1173K (900˚C) microstructure contain micro sized rod shaped precipitates (B2 order structure) and the corresponding stress strain curve showed no yield drop along with large work hardening rate indicate that dislocations are no longer cutting through the particles, instead accumulate in the form of tangles around them. Stress- strain curves corresponding to the three conditions are shown in Figure 2.5.
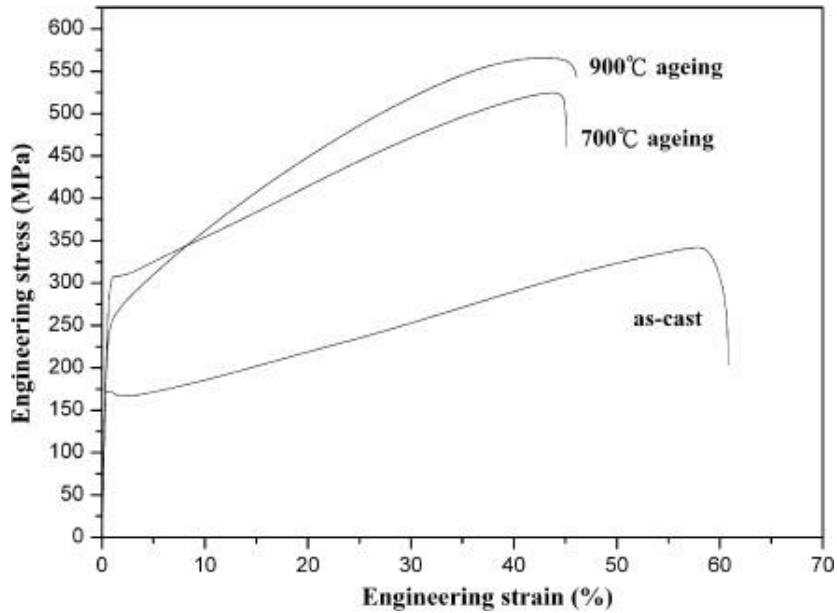
Figure 2.5 Stress- Strain behavior of $Al_{0.3}$CoCrFeNi HEA in as-cast and aged at 973K (700˚C) and 1173K (900˚C) [24]

Qiao et al., [25] studied deformation behavior of single phase BCC AlCoCrFeNi HEA in compression mode in the temperature of 278 K to 77 K- and showed that the yield strength and fracture strength increases by 29.7% and 19.9%, respectively with decreasing the temperature from 298 to 77K. as shown in figure 2.6, without significant change in fracture strain. However, there is a change in the fracture mode from inter-granular at 298 K to trans-granular at 77 K.
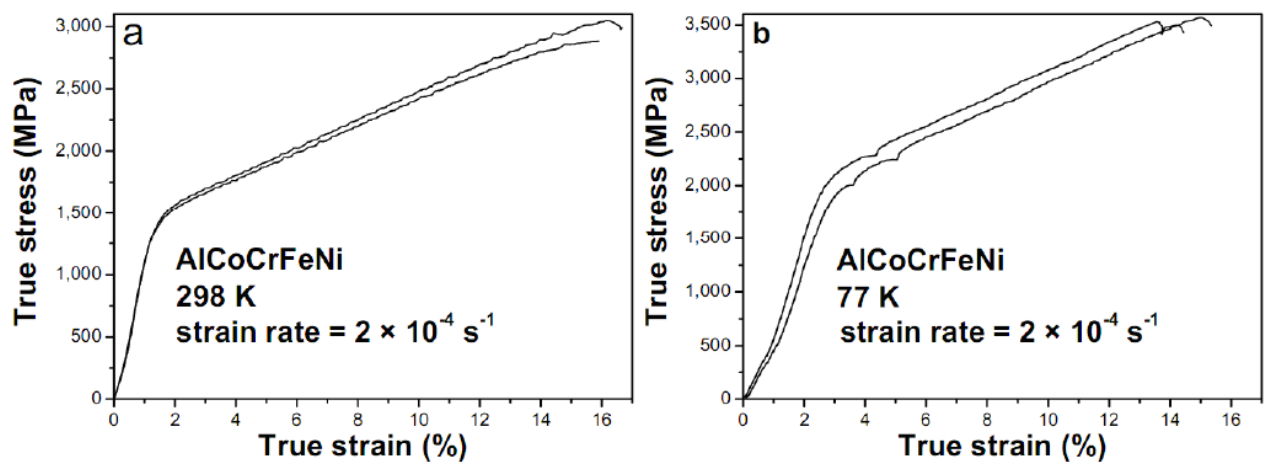
Figure 2.6 Compressive true stress and true strain curve of AlCoCrFeNi HEA at 298K and 77K [25]

9

Laktionova et.al., [26] reported deformation studied on $Al_{0.5}CoCrFeNi$ alloy in the temperature range of 300K to 4.2K shown in figure 2.7 and exhibited yield stress of 450 MPa and 750 MPa at temperatures 300K and 4.2K respectively. Sample deformed at temperature below15 K showed serrated behavior, indicates the change in deformation mechanism below 15K temperature.
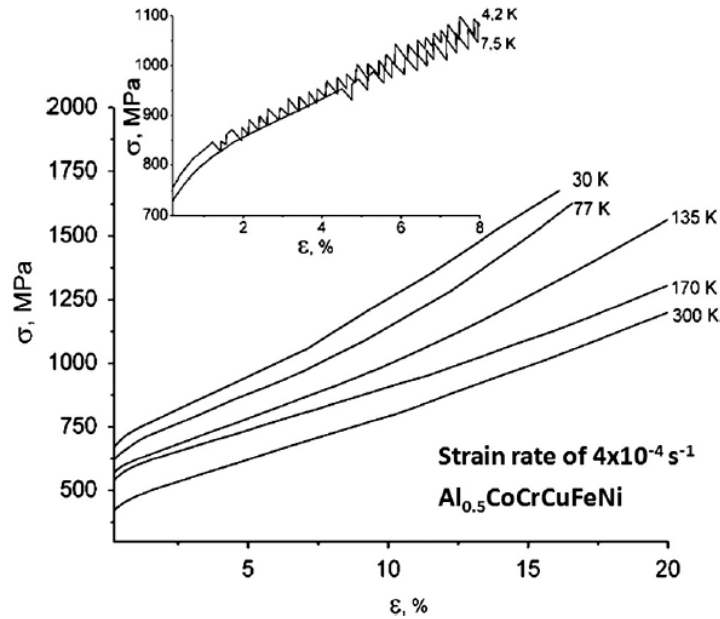
Figure 2.7 Compressive stress strain curve of $Al_{0.5}CoCrFeNi$ alloy tested in the temperature range of 300 K to 4.2 K. Inserted figure shows the serrated behavior at temperatures below 15 K [26]

S.G.Ma et al., [27] investigated the tensile behavior of $Al_{0.3}CoCrFeNi$ HEA single crystal with <001> orientation grown using Bridgman technique and compared to the as cast alloy as shown in figure 2.8. It is observed that, the yield strength and UTS of single crystal are lower than as-cast by 32 % and 24 % respectively. Whereas as-cast condition exhibit limited ductility as compared to single crystal, more than 80% of tensile elongation. TEM analysis showed the presence of dislocation bundles in single crystal HEA and these are responsible for strain hardening in the single crystal during deformation and results in higher ultimate tensile elongations.
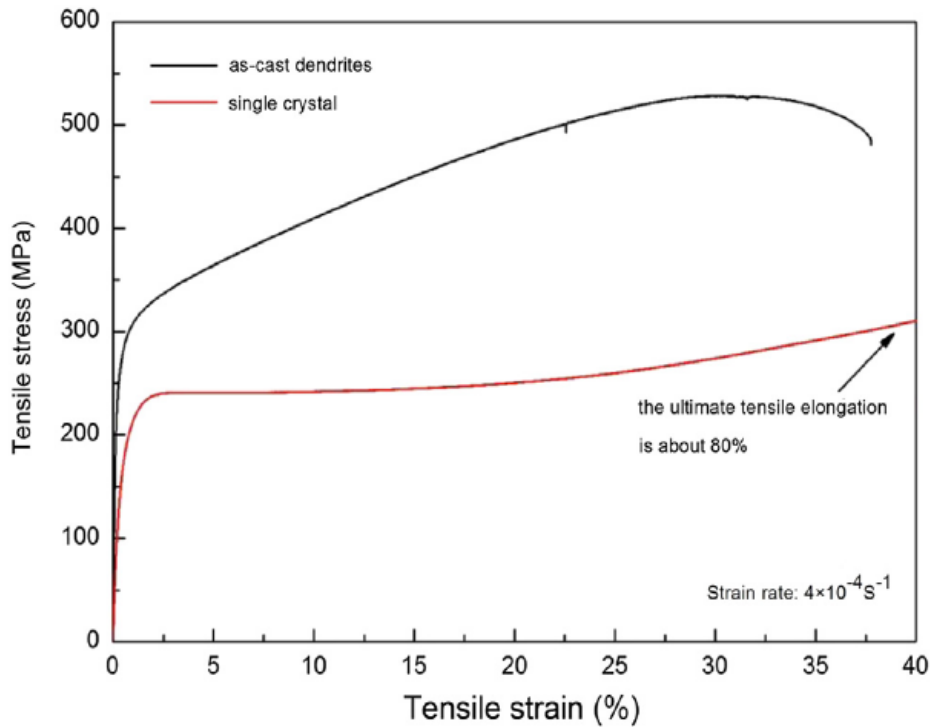
Figure 2.8 Stress –strain graph of as-cast and single crystal $Al_{0.3}CoCrFeNi$ HEA [27]

Dongyue LI et al., [28] investigated the tensile flow behavior of $Al_{0.3}CoCrFeNi$ HEA fibers with different diameter fabricated by hot-drawing. The microstructure of post processed (hot drawing) shows presence of nano-sized B2 precipitates in FCC matrix. Tensile experiment were conducted at temperature 298K at different strain rates: $10^{-3}s^{-1}$, 2 x $10^{-4}s^{-1}$, 5 x$10^{-5}s^{-1}$; and at temperature 77K at strain rate 2 x$10^{-4}s^{-1}$. Figure 2.9 shows both strength and ductility are more in fibers tested at 77K than fibers tested at 298K.The post deformed microstructures showed formation of deformation induced nano-twin in fibers tested at 77K which may be reason for observed greater strength and elongation in fiber tested at 77K.
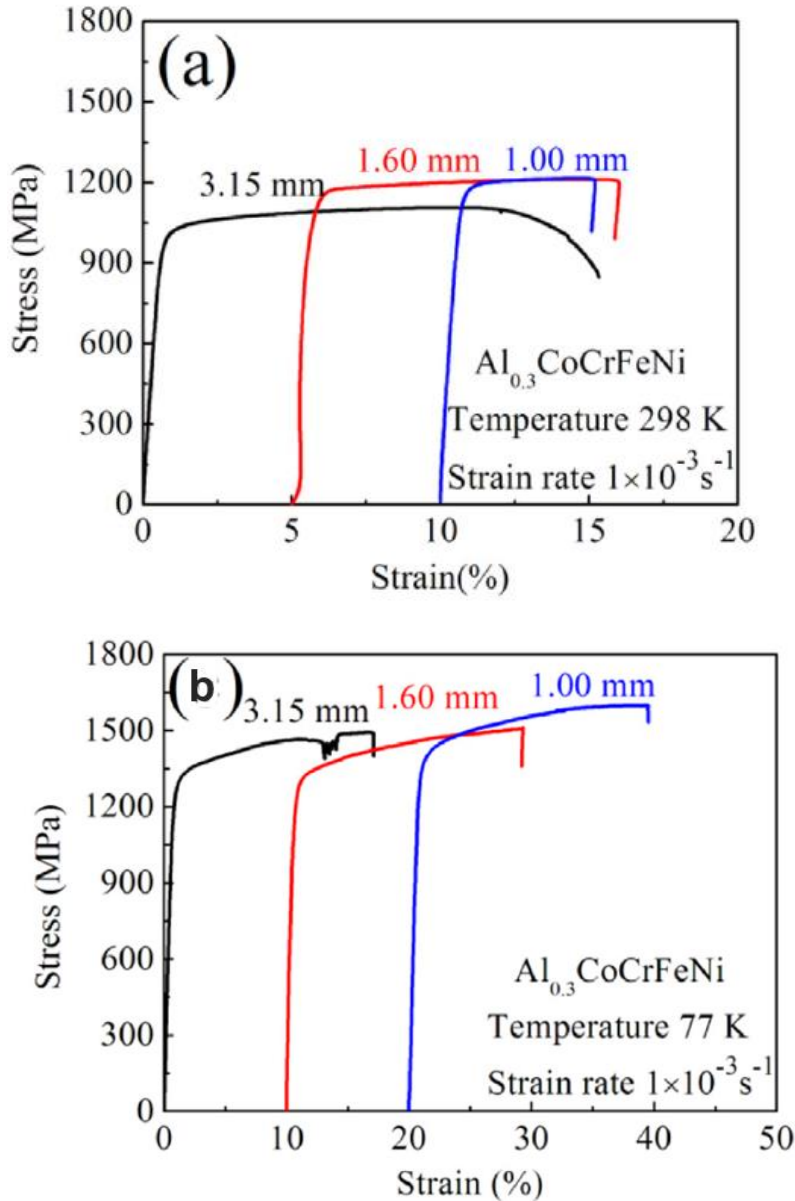
Figure 2.9 Tensile flow curves of Al$_{0.3}$CoCrFeNi HEA fibers with different diameter at temperature a) 298K and b) 77K [28].

All these studies mainly focused on understanding the deformation behavior of HEAs in compression mode and tensile mode at quasi-static strain rate at temperatures ranging from cryogenic to room temperatures. Unfortunately, at low temperatures HEAs in as-cast condition have limited formability. Formability especially super-plasticity is major concern for forming industries to produce complex curved components to use in automotive, aerospace and other applications.

Most of the studies discussed above are focused more on strength. Maximum uniform elongation reported in in the range of 80 % [27] in single crystal HEA. Since, HEAs are good alternative alloys to the conventional alloys, it is necessary for these alloys to exhibit good ductility to process them into components with complex shapes. In this scenario, it is necessary to study the possibility of superplastic behavior in these HEAs.

2.3 Super-plasticity:

Super-plasticity is the ability of material to exhibit very large uniform elongations without failure and it is important to produce complex, curved shapes that are near to final dimension, thereby minimizes the scrap produced and also reduce machining time. In addition, it lowers the amount of material used, thereby reduces the total material cost. The basic conditions for the superplasticity are fine stable equi-axed grains, high strain rate sensitivity, high temperature and resistance to cavitation.

2.3.1 Microstructural Prerequisites:
1)Fine Grain Size:

Extensive experimental data shows that Grain boundary sliding (GBS) is the dominant deformation process in superplastic materials which is defined as the sliding of the one grain over the other along the common grain boundary [29] [30] [31]. To increase the contribution of grain boundary sliding to the total strain, it is essential to have more grain boundaries present in the material which can be possible by lowering the grain size. When GBS is the controlling deformation process, the strain rate and the grain boundary sliding strain is inversely proportional to the grain size of the material (Eq 3) [29] [30]. Literature suggests that, material to exhibit superplasticity should have grain size less than 10 µm.

$$\dot{\varepsilon} \; \alpha \; d^{-p} \text{………………...…..} \text{Eq (3)}$$

where is the $\dot{\varepsilon}$ Strain rate , d – is the grain size of the material, p is the grain size exponent which can vary between 1 and 2 depending on the accommodation mechanism for grain boundary sliding.

One way of decreasing the grain size is by suitable thermomechanical processing.

2) Nature of second phase:

Fine grained microstructure has to be stable during deformation at high temperature to produce superplasticity. Fine and uniform distribution of the second phase or particles along the grain boundaries can pin the grain boundaries thereby inhibit the grain growth. And the relative strengths of the parent and second phase is also main parameter to control prior failure of the material during superplastic flow by cavity formation [32]. The interface between parent and second phase act as a preferential site for crack nucleation or cavity formation due to incompatible deformation or lack of proper accommodation mechanism. Thus the second phase should have similar to the parent phase. If the second phase is considerably harder than the parent phase, then it should be fine and uniformly distributed.

3) Grain boundary nature:

As mentioned in the previous section, grain boundary sliding is the dominant mechanism for superplastic deformation. Grain boundary sliding is easy in case of high angle boundaries as compared to low angle and special boundaries [29]. Materials containing low angle grain boundaries can also behave superplastic by converting the low angle grain boundaries as high angle grain boundaries by thermal or thermo-mechanical processing. Superplasticity can also achieved in some alloys with low angle grain boundaries. In these alloys continuous recrystallization takes place during deformation so that the low angle grain boundaries are converted to high angle grain boundaries in the initial stage of deformation and these high angle grain boundaries contributes to subsequent grain boundary sliding(GBS), leads to superplastic flow.

2.4 Superplasticity in HEAs:

Recent experiments on HEAs have shown that these alloys can also exhibit superplastic flow when tested at elevated temperatures.

Kuznetsov et al., [33] studied the microstructure and deformation behavior of hot forged AlCoCrFeNi alloy in tensile mode at high temperatures shown in figure 2.10. Grain refinement by multi axial forms duplex structure with grain size in the order of 1.5μm and tested in the tension in the temperature range of 700°C (973K) to1000°C (1273K) and strain rates range of 10^{-2} s^{-1} to 10^{-4}s^{-1}, and the maximum elongation to failure of 864% was observed at 1000°C (1273K) temperature and 10^{-2} s^{-1} strain rate. The post deformation microstructures showed no change in either grain size or morphology.
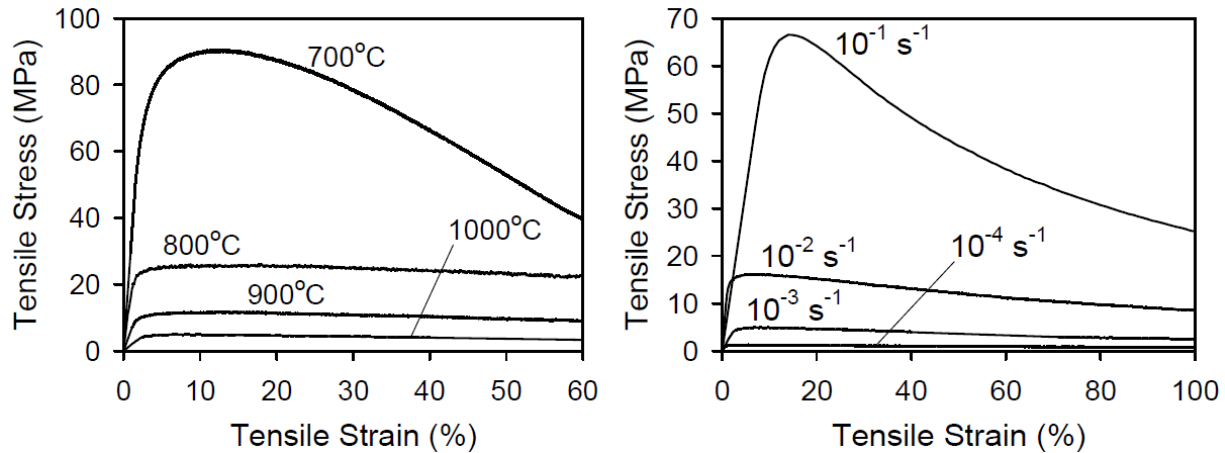
Figure2.10 Tensile stress-strain graphs of AlCoCrCuFeNi alloy processed by hot forging at a)10^{-3}s^{-1} at temperatures 700°C - 900°C (973K - 1073K) b) temperature 1000°C (1273K) at 10^{-1}s^{-1} - 10^{-4}s^{-1} [33].

Hamed shamir et al., [34] reported the tensile flow behavior of CoCrFeNiMn alloy with a grain size of 10 μm processed by high pressure torsion at room temperature. Tensile experiments were conducted in the temperature ranging of 773 K to 1023 K and at different strain rate as shown in figure 2.11. It is observed that deformation at 973 K exhibits superplastic elongation of 600% temperature at 10^{-3} s^{-1} strain rate. Post deformation microstructure suggesting that the superplastic elongation is due to the formation of fine precipitates along the grain boundaries which are inhibiting the grain growth during superplastic deformation.
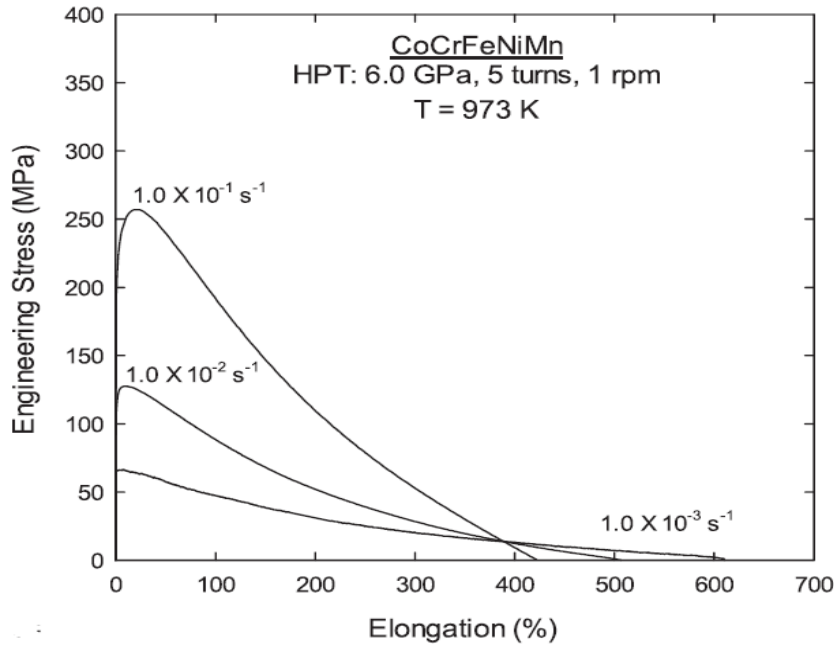
Figure 2.11 Flow curves for samples processed by HPT AT 973 K and at different strain rates [34].

Hamed Shahmir et al., [35] also reported the effect of titanium on the superplastic ductility of CoCrFeNiMn HEA processed by high pressure torsion (HPT) at room temperature. The addition of Ti favored precipitation formation. Samples are tested in temperatures range of 873 to 1000K and showed the maximum elongation to failure 830% at 973K temperature and $10^{-2}s^{-1}$ strain rate. From the results it is clear that addition of titanium increases the superplastic elongation in CoCrFeNiMn HEA.

Reddy et al., [36] investigated the high temperature plastic deformation behavior of thermo-mechanically processed quasi-single phase CoCrFeMnNi alloy having a grain refinement of 1.4 μm grain size. The true stress vs elongation curve was shown in figure 2.12. At room temperature and $10^{-3}s^{-1}$ strain rate, alloy exhibit 1050 MPa yield stress and only 35% of elongation. Whereas, deformation at 1023K and $10^{-3}s^{-1}$ strain rate the comparatively very low yield stress but ductility increases to 160%. The maximum elongation to failure of 320% was observed at 1023K temperature and 10^{-4} s^{-1} strain rate.
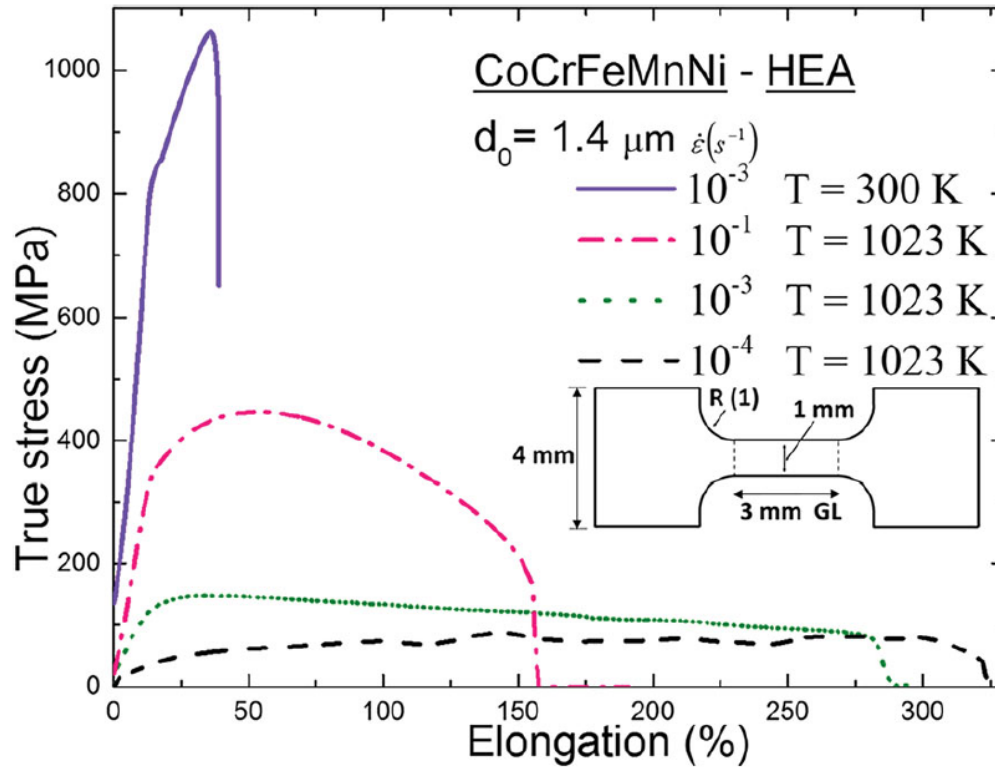
Figure 2.12 True stress- elongation curve of CoCrFeMnNi at 300K and 1023 K at different strain rates [36].

.

Composition	Processing	Temperature (K)	Strain rate (s^{-1})	Max. Elongation (%)	Ref
AlCoCrCuFeNi	Hot Forging	1273(1000°C)	10^{-3}	860	Kuznetsov et al[33]
CoCrFeNiMn	HPT	973(700°C)	10^{-3}	600	Shahmir et al. [34]
CoCrFeNiMnTi$_{0.1}$	HPT	973(700°C)	10^{-2}	830	Shahmir et al. [35]
CoCrFeNiMn	Rolling	1023(750°C)	10^{-4}	320	Reddy et al. [36]

Table 1 Experimental conditions and superplastic elongations of HEAs.

Table 1 summarizes the available maximum elongation to failure reported in the literature in different HEAs deformed at high temperatures. From the literature study, it is clear that HEAs have ability to exhibit superplastic flow behavior, after grain refinement.

2.5 Objective:

1). To study the microstructure evolution and stability of cold rolled $Al_{0.3}CoCrFeNi$ HEA annealed at different temperatures and annealing times.

2). To understand the effect of temperature and strain rate on flow behavior of the thermo-mechanically processed $Al_{0.3}CoCrFeNi$ HEA.

3). Explore the possibility of superplastic behavior of $Al_{0.3}CoCrFeNi$ HEA.

2.6 Why $Al_{0.3}CoCrFeNi$ HEA:

$Al_xCoCrFeNi$ HEAs shows variation in microstructure from FCC to BCC with addition of Al content. The large atomic size of Al in turn changes the lattice parameter causes high strains in crystal lattice and leads to phase transformation from FCC to BCC. At x=0 to 0.5 it has FCC structure, little increment in Al content in the range from x=0.5 to 0.9 both FCC, BCC structures co-exist. Further addition of Al more than x=0.9 completely stabilizes the BCC structure. [37].

$Al_xCoCrFeNi$ can be strengthened by precipitate formation. Precipitate formation can be enhanced by prior deformation followed by annealing. Deformation increases the defects which are nucleation sites for precipitation. Thermo-mechanical processing of $Al_{0.3}CoCrFeNi$ forms $L1_2$ (ordered FCC) precipitates having stoichiometry Ni_3Al due to high negative enthalpy of bond formation between Ni and Al (decreases free energy). However, these $L1_2$ precipitates are stable in temperature range of 500°-700^oC. At temperatures 700^oC-1000^oC B2 precipitates having stoichiometry NiAl replaces L12 precipitates. The stability of precipitates depends on interplay among interfacial, chemical and elastic energies. The interfacial energies between parent phase and precipitates are: FCC/L12 – 0.015 J/m^2, FCC/B2 – 0.2 J/m^2. The driving force due to large amount

of deformation energy produced during cold rolling and the higher number of Al-Ni unlike bonds per atom in B2 structure compared to L12 structure stabilizes B2 precipitates. $Al_{0.3}CoCrFeNi$ was homogenized at 1200C to get single phase FCC structure. Cold rolling of single phase (annealing at temperature above 1200 C produces single phase FCC) FCC phase followed by recrystallization can produce fine eqi-axed grain size. Subsequent formation of the B2 phase along grain boundaries and triple junctions stabilize this fine grain size at high temperature which can be a suitable condition for superplastic deformation and this is the strategy followed in the present work [38] [39].

Most of the automotive and aerospace component are fabricate by superplastic forming technique. At present 30-40% of components in these applications are made from Aluminum and Titanium alloys due to their light weight and high specific strength which will increase the fuel efficiency. Recent studies on HEAs shows that the addition of Al decreases the density of AlxCoCrFeNi alloys (approximate density ~ 6.5g/cc). Ashby map; plotted yield strength against density shown in Figure 2.13 clearly suggesting that AlxCoCrFeNi alloys have high specific strength comparable to Aluminum and Titanium alloys and can be a good alternative structural material for automobile applications.
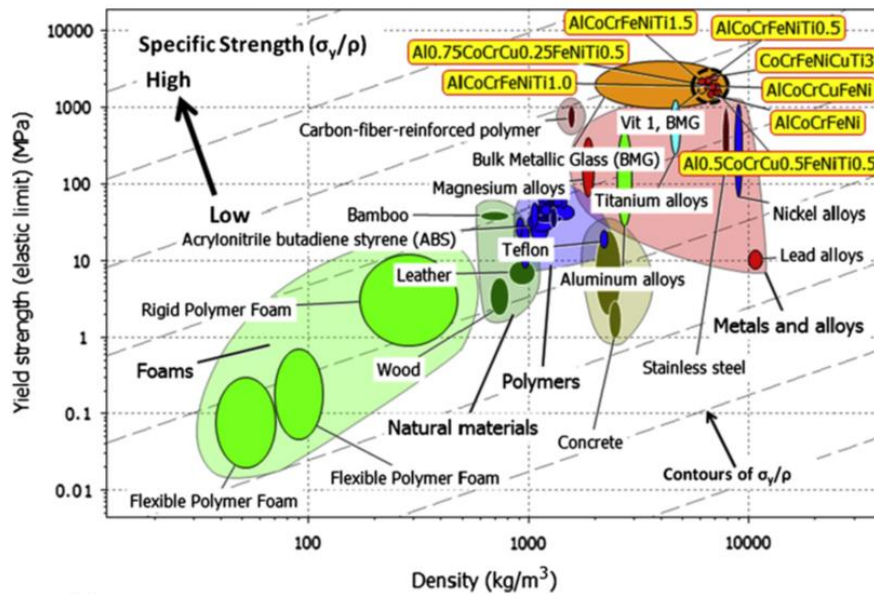
Figure 2.13 Ashby map: yield strength vs density.

Chapter 3: Experimental Procedure

This chapter discusses about the experimental procedures adopted during the present work.

3.1 Materials and Methods:

$Al_{0.3}CoCrFeNi$ (molar ratio) ingot was produced using vacuum induction melting of pure metals (purity of >99wt%). The ingot was homogenized at 1200°C for 5hr followed by surface machining to remove blow holes and porosity. The machined ingot was soaked at 1100°C for 2 hrs prior to forging and intermediate soaking was done for 1 h. Forging was done using 1000 T hydraulic press through upsetting and drawing operation with a reduction of 35% per press. Forged block was hot rolled at 1050°C to a thickness of 6 mm and width of 100 mm which is the starting material for the present study. The schematic representation of the work in the form of flow chart is shown in Figure 3.1.
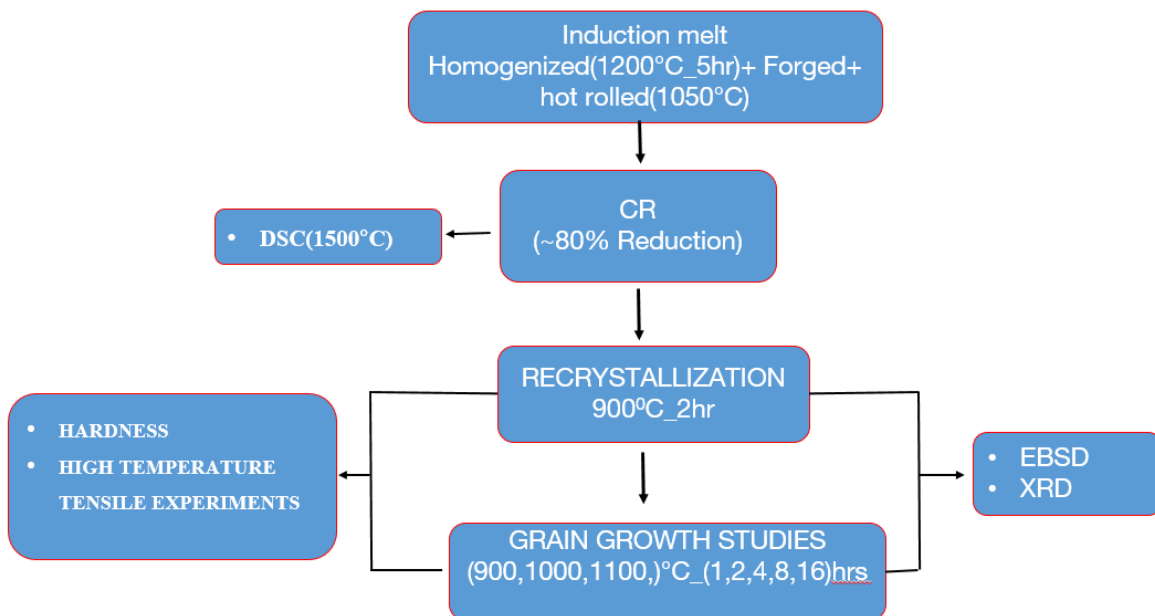
Figure 3. 1 Experimental Flow chart

3.1.1 Sample preparation:

Surface of the hot rolled sheet was cleaned by surface grinding and cut into small pieces with dimensions: 40 x 20 x 5.3 mm using Secotom precision cutting machine and subsequently cold rolled to 80% reduction in thickness using a laboratory-scale two high rolling mill with a roll diameter of ~ 140 mm (SPX Precision Instruments, Fenn Division, USA) in multiple passes, approximately 2% reduction in each pass.

3.1.2 Compositional analysis:

Sample for chemical composition analysis are collected from the as received hot rolled sheet in the form of drilling chips and the compositional analysis was done using Inductively Coupled Plasma Mass Spectrometry (ICP-MS) which is capable of detecting metals and several non-metals at concentrations as low as parts per billion on non-interfered low-background isotopes.

3.2 Microstructural studies:

3.2.1 Metallography:

Samples for microstructural analysis are initially polished with silicon carbide (SiC) emery papers in a sequence of 320, 500, 800, 1000, 2000, and 3000 grid size. Further final polishing was done on soft polishing cloths using colloidal Alumina till scratch free surface was obtained. Polishing was carried out by using rotating disc machine (ATM polishing machine). Polished samples were cleaned thoroughly with running water. Further cleaning was done by ultrasonicator in acetone to remove the alumina particles from the sample surface. The cleaned samples were etched with the aquaregia (HCl : HNO_3 in 3:1 ratio) for 40-50 Sec to reveal the microstructure. Microstructural was examined using LEICA optical microscope as shown in Figure 3.2, which is coupled with imaged analysis software.
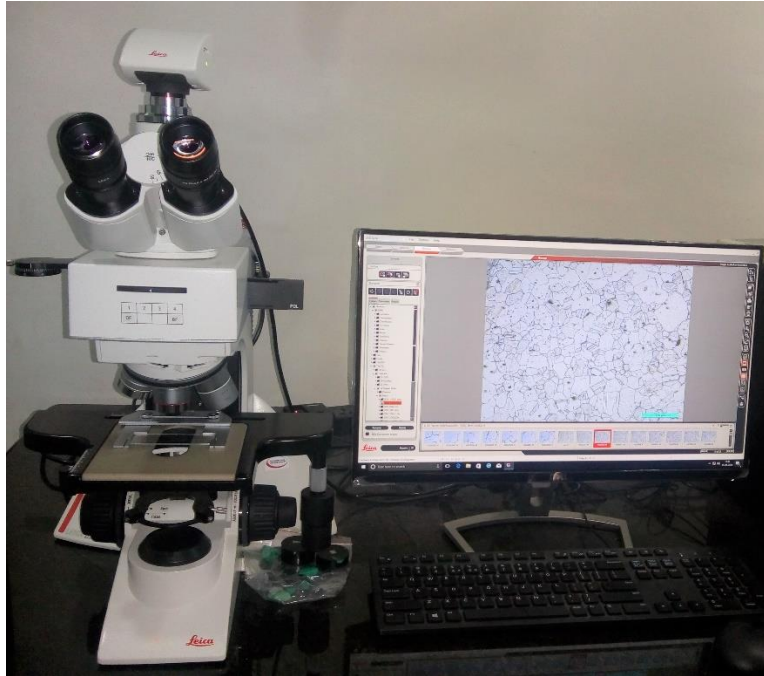
Figure 3.2 Optical Microscope

3.2.2 Scanning Electron Microscopy:

The cold rolled plates are annealed at 900°C for 2hr for recrystallization. Recrystallized samples were used to study the microstructural evolution at 900, 1000, 1100°C temperatures for different times (1hr,2hrs 4hrs,8hrs and16hrs). The isothermal heat treatment done in tubular furnace with inert Argon atmosphere.

The microstructure of the annealed samples was characterized using SEM-EBSD (Scanning Electron Microscopy-Based Electron Backscattered Diffraction) which is shown in Figure 3.3. For EBSD investigation, annealed samples were initially mechanical polished till 1μm using by emery papers and alumina. Mechanical polished samples were electro polished at -5°C and 18-20 V for 6 to 8 seconds using the following electrolyte: 90% methanol + 10% perchloric acid.

Carl Zeiss FEG SEM was used along with Oxford instrumentation EBSD camera to get EBSD data. The Aztec-HKL software (Oxford Instruments, UK) was used for data acquisition. Data was further analyzed using TSL-OIM^{TM} software (EDAX Inc., USA).

The chemical composition of individual phases present in microstructure is obtained using Energy-dispersive X-ray spectroscopy(EDS). Fracture tip of the failed tensile samples are examined using SEM.

Figure 3.3 Scanning Electron Microscopy

3.1 Mechanical Testing:

3.1.1 Vickers hardness:

Samples for hardness measurement are prepared by polishing using silicon carbide (SiC) emery paper up to 2000 grid size until scratch free surface is achieved. Polished samples were cleaned thoroughly with running water. Hardness of the polished samples were measured using computer-controlled Macro Vickers hardness machine at 0.3 Kgf load with 15 secs as dwell time. During hardness measurements, care had been taken to cover minimum 4 to 5 grains under the indenter. More than 20 measurements were made in each condition to get the mean hardness. The approximately 4 to 5 grains were covered under the indentation.

3.3.1 Tensile Testing:

Flat dog bone shaped, as shown in Figure 3.4, tensile specimens were cut from the annealed strip using electro-discharge machine(EDM) parallel to the rolling direction. The room temperature tensile tests were performed at a strain rate $1\text{x}10^{-3}\text{s}^{-1}$ using a 30kN capacity computer controlled universal testing machine (Instron, U.S model number:5967). Dog bone shaped tensile samples were coated with white and black paint using spray gun to form speckle pattern as shown in Figure 3.5. Images of the dog bone shaped tensile sample fixed between the pull rods are captured continuously with a time interval of 500 milli-seconds using Camera (Nikon ED, AF MICRO NIKKOR 200mm 1:4D, model: Grasshopper3 GS3-U3-89S6M) attached with appropriate filters. Captured images were further processed to calculate the strain using Vic-2D digital image correlation (DIC) software. DIC compares a series of captured grey-scale images with a reference pattern, track pixel movement in the region of interest and calculates 2D displacement and strain fields using a correlation algorithm.

To perform high temperature tensile test, three zone ATS furnace was attached to the same Instron (U.S model number:5967) universal testing machine as shown in the figure 3.6, Port hole with 10 x 2 cm dimension is provided at the middle of the furnace to capture the sample images during high temperature deformation to measure the strain using DIC. However, because of the problem with paints at high temperature, DIC was not used for high temperature tensile experiments to get the strain information. Strain at high temperature are calculated using cross head displacement. Tests were carried out with an initial strain rates ranging from 10^{-1} to 10^{-4} s^{-1} at different temperatures: 400, 600, 700 and ,800$^{\text{o}}$C. The tensile samples were heated from room temperature to desired temperature at 50$^{\text{o}}$C/min heating rate and soak at the test temperature for 20 min before starting the test. Thermocouple was inserted close to the sample to measure the sample temperature during experiment. The load applied along the rolling direction. At least two samples were tested for each condition to get repeatability and the corresponding average values were reported.
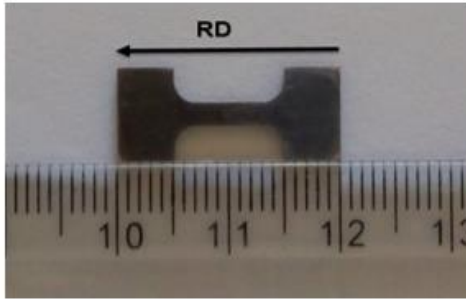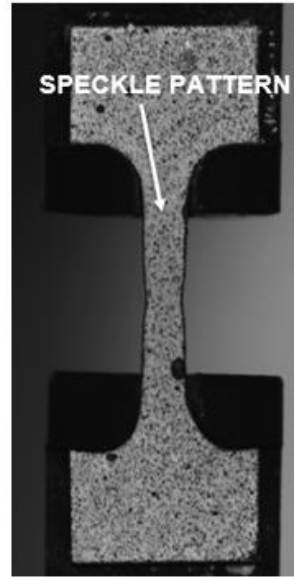
Figure 3.4 Tensile specimen   Figure 3.5 Tensile specimen with speckle pattern
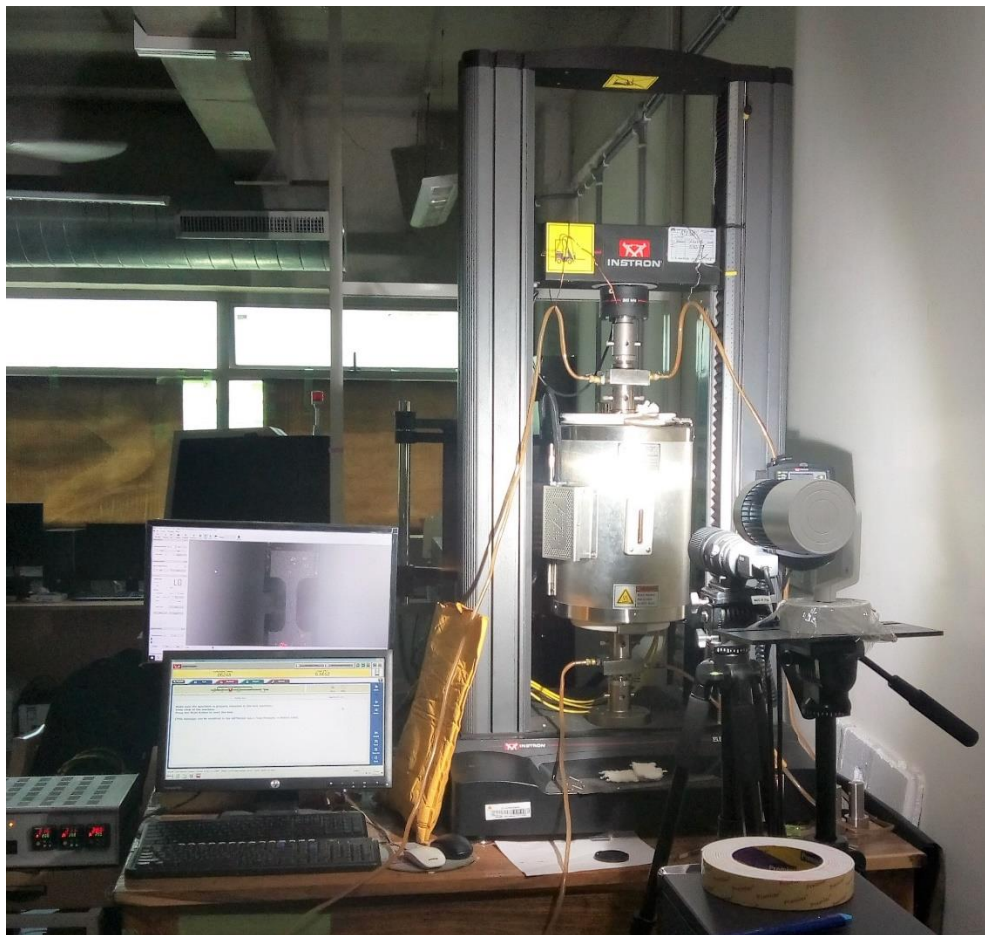
Figure 3.6 Instron attached with three zone ATS furnace

Chapter 4: Results and Discussions

Current chapter is focused on results obtained through different experiments starting with the microstructural evolution during annealing, compositional analysis of the phases (SEM- EDS) hardness tests and high temperature tensile data and finally presented the fracture surface morphology. The results were analyzed simultaneously with proper justification.

4.1. Microstructural Evolution:

The microstructure of the as received condition (hot rolled and homogenized), shown in figure 4.1, consists of significant amount of annealing twins. Composition of the alloy was analyzed using both ICP-MS and SEM-EDS and are listed in table2 clearly suggesting that both the methods show almost similar composition.

Sample cold rolled to 80% reduction in thickness is studied using differential scanning calorimetry (DSC) with a heating rate of 5°C/min (Fig 4.3) and there is no phase transformation observed except melting at ~1400°C. Cold rolled samples were annealed at 900°C for 2 hours in argon atmosphere and the corresponding EBSD phase map is shown in Figure 4.4a. The EBSD image shows the fully recrystallized and equi-axed, fine grained structure with precipitates (secondary phase) along the grain boundary and especially at triple points. And also noticeable amount of twins were observed. The measured grain size of the recrystallized condition is 3.2 µm. The grain size measurements were performed by using mean linear intercept method shown in figure 4.2 using sigma scan pro image analysis and minimum 500 grains were measured in each condition.

Elements	Composition in atomic %	
	FESEM_EDS	ICP_MS
Al	8.0	8.3
Co	22.5	22.7
Cr	24.3	23.4
Fe	25.0	23.9
Ni	20.2	21.7
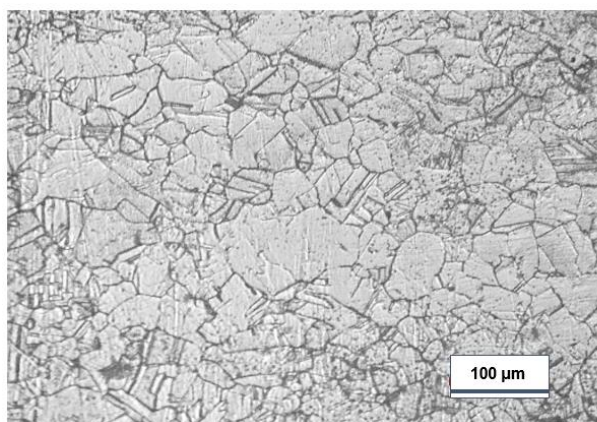
Figure 4. 1 Microstructure of as received material   Table 2. EDS and ICP-MS composition analysis
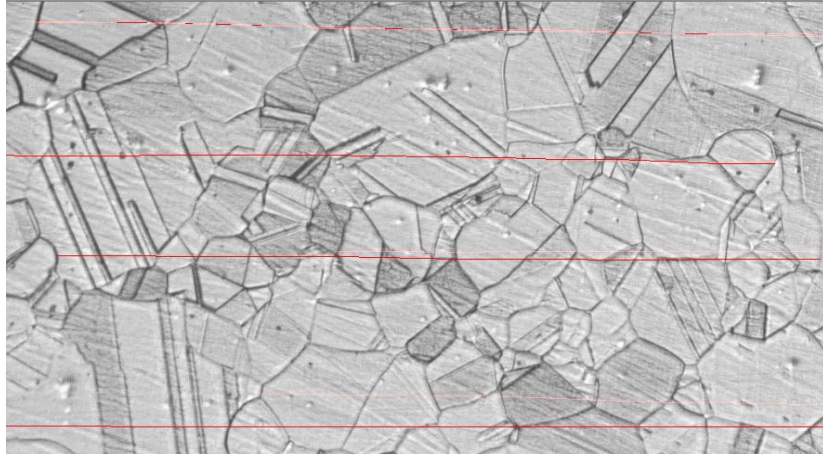
Figure 4.2 Grain size measurement using linear intercept method
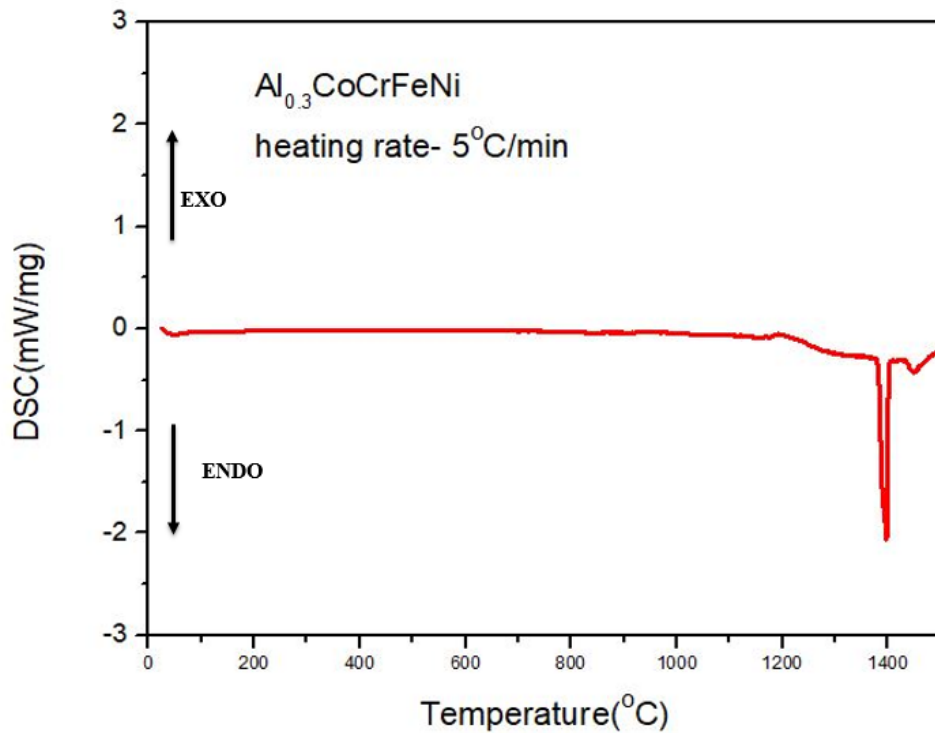
Figure 4.3 DSC curve of Al0.3CoCrFeNi alloy after cold rolling to 80% reduction in thickness

The recrystallized sample (annealed at 900°C for 2hr) was taken as starting material for further microstructural studies and are annealed at different temperatures 900, 1000 and 1100°C for different time intervals: 1, 2, 4, 8, and 16hr and the corresponding EBSD phase maps are shown in Figures (4.4 to 4.6).

Rolling Direction →

a) Recrystallized (900°C_2hr)   b) RC+900°C_1hr   c) RC+900°C_4hr   d) RC+900°C_6hr
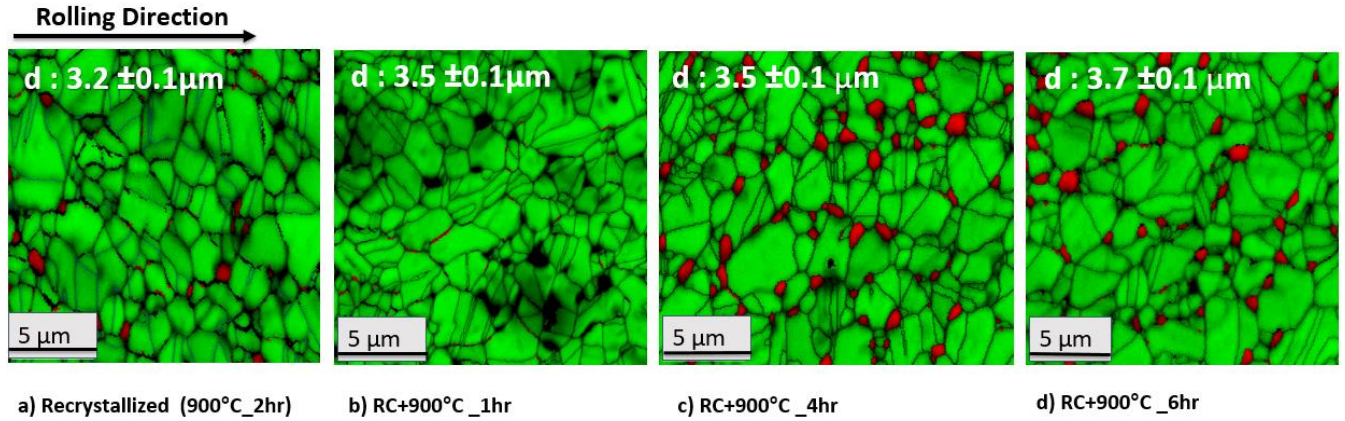
Figure 4.4 a) EBSD phase maps of fully recrystallized sample at 900ºC for 2hrs, (b-d) microstructure evolution of recrystallized sample annealed at 900ºC for different time intervals.
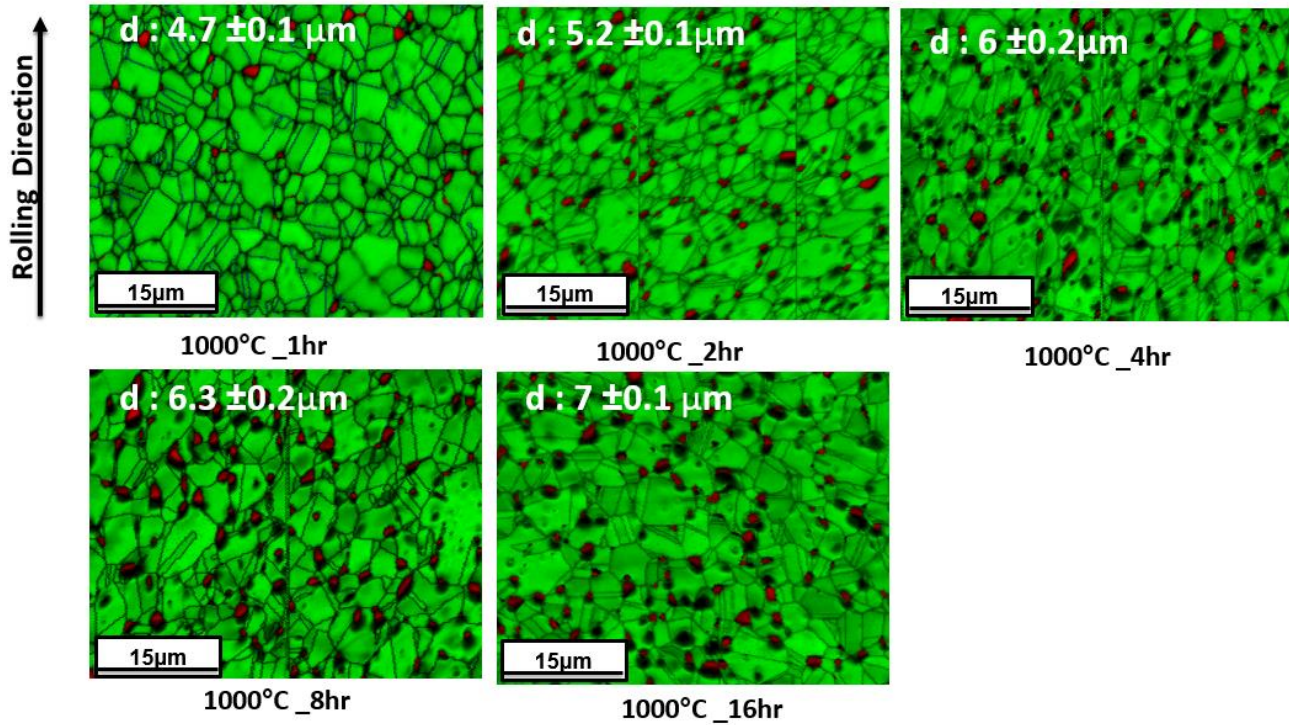
Figure 4.5 Microstructure evolution of recrystallized sample annealed at 1000°C for different time intervals.
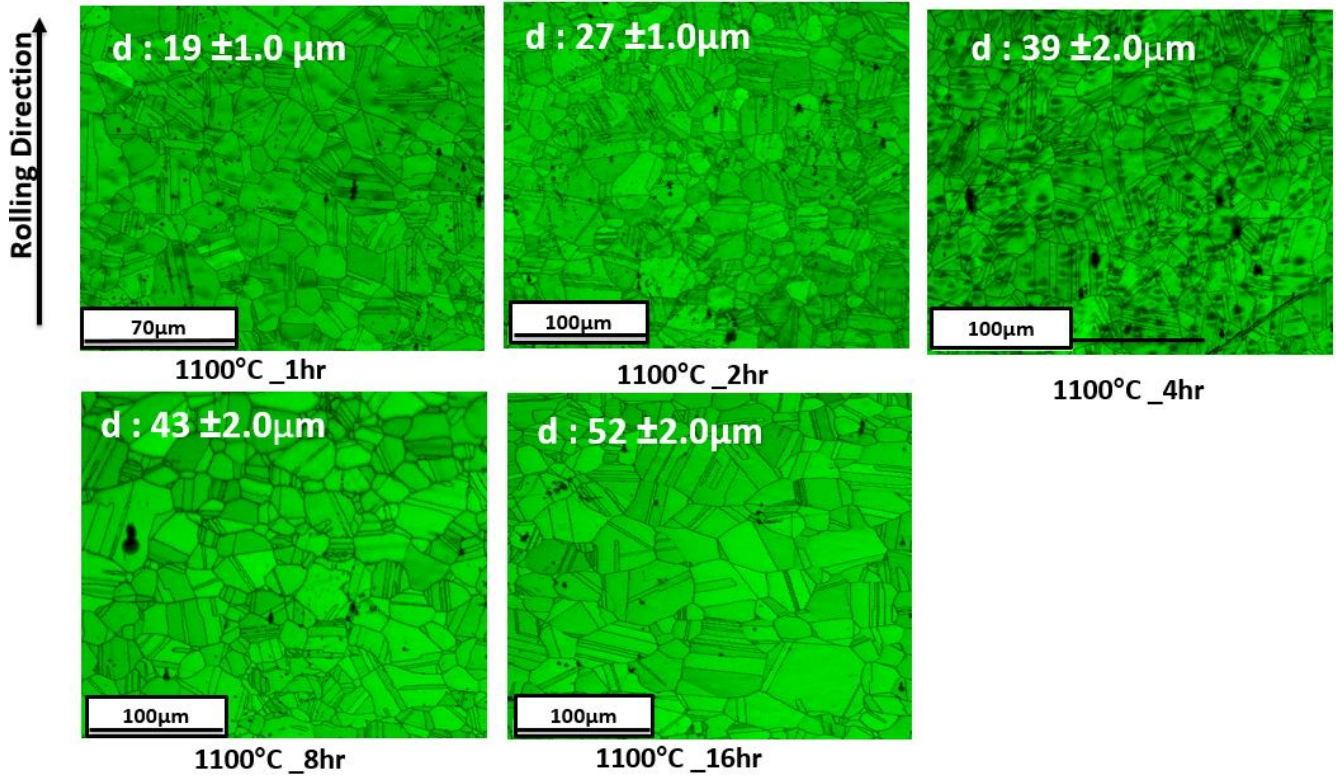
Figure 4.6 Microstructure evolution of recrystallized sample annealed at 1100°C for different time intervals.
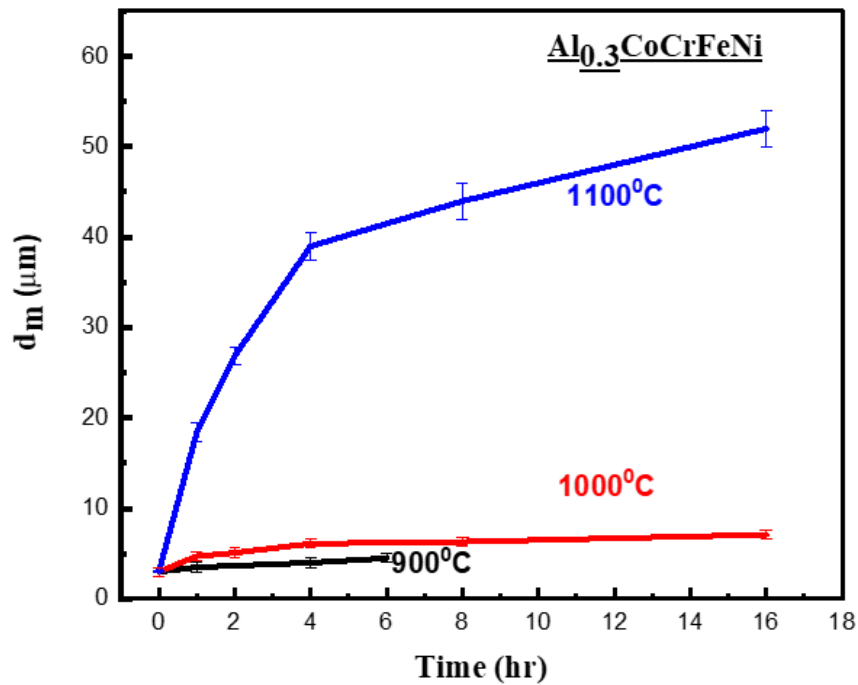
Figure 4. 7 Variation of grain size of parent FCC phase with annealing temperature and time in Al $_{0.3}$CoCrFeNi HEA

Figure 4.4 - 4.6 show the EBSD images shows the microstructure of $Al_{0.3}CoCrFeNi$ HEA after annealing at temperatures from 900℃ to1100℃ for 1-16 hrs. The FCC and BCC phases were indicated with green and red colors, respectively. And the high angle grain boundaries and annealing twin boundaries ($\Sigma 3$ 60° $<111>$) were indicated by black colored lines. The microstructures at 900℃ and 1000℃ clearly reveals the evolution of equi-axed, fine grained microstructure along with BCC phase at grain boundaries and especially at triple points. But in contrast, coarse grains without BCC phase was observed in samples annealed at 1100℃.

The grain size (d_m) variation with annealing time and temperature is shown in figure 4.7 suggesting that there is no significant increment in the FCC matrix grain size (d_m) with either increasing the annealing temperatures from 900 to 1000℃ or with annealing time from 1 to 16hr. However, further increasing annealing temperature to 1100℃ shows rapid grain coarsening. Therefore, it clearly indicates that the presence of precipitates at grain boundaries strongly suppress the grain boundary migration by pining the grain boundaries and results fine, equi-axed, stable grain size in FCC parent phase.
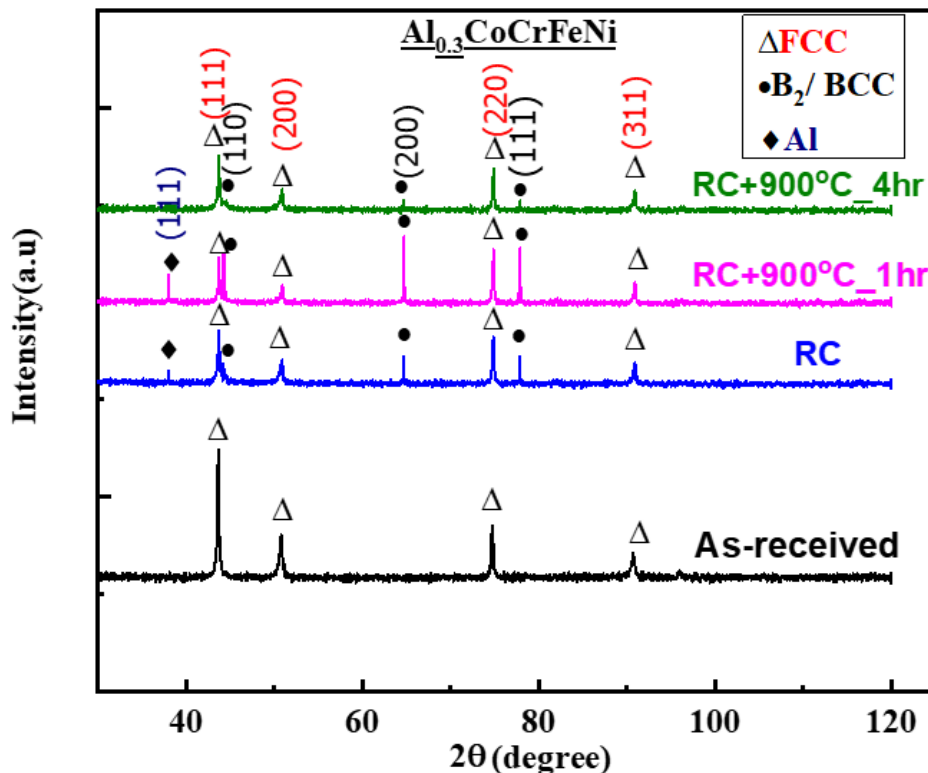
Figure 4.8 XRD pattern of $Al_{0.3}CoCrFeNi$ HEA in as-received, recrystallized and annealed conditions

Figure 4.8 showing the XRD data in as received, recrystallized and annealed at 900 o C for 1 and 4hr conditions. As received material showing only FCC phase whereas both recrystallize and annealed for 1 and 4hr samples having both FCC and BCC phase. It further conforms that second phase is forming during heat treatments. Interestingly pure Al peak was observed in the annealed conditions. The average chemical composition of FCC parent phase and BCC phases were measured using EDS (corresponding BSE image shown in figure 4.9) as $Al_{3.7}Co_{23.6}Cr_{26.9}Fe_{26.6}Ni_{19.3}$ and $Al_{16.4}Co_{18.9}Cr_{17.9}Fe_{19.3}Ni_{27.4}$, respectively (table 2). The chemical composition of the phases shows that the second phase is rich in Al and Ni.
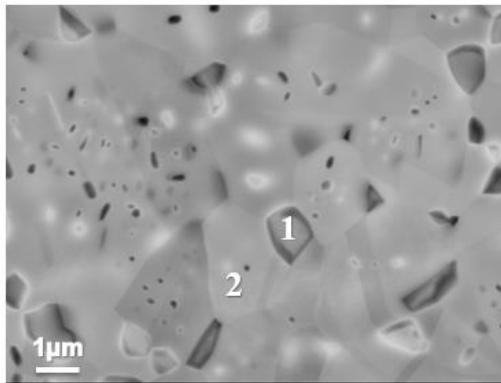
ELEMENT	COMPOSITION (At%)	
	SPOT 1(B2/BCC)	SPOT 2(FCC)
Al	16.4	3.7
Cr	17.9	26.9
Fe	19.4	26.5
Co	18.9	23.6
Ni	27.4	19.3

Figure 4.9 BSE images of $Al_{0.3}CoCrFeNi$ HEA sample annealed at 900^oC for 4hrs

Table 3 compositional analysis of FCC and BCC phases
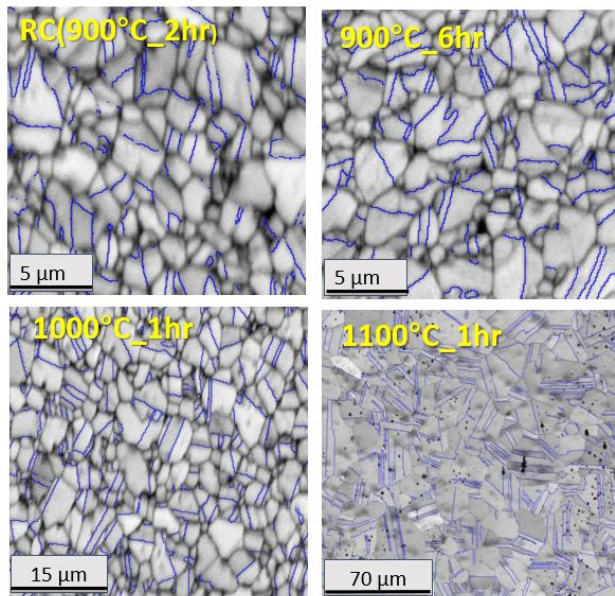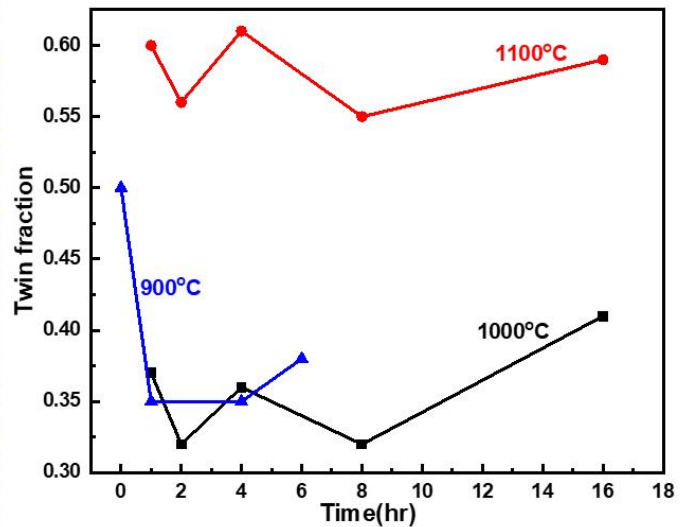
Figure 4.10 a) EBSD grain boundary map of $Al_{0.3}CoCrFeNi$ HEA samples annealed at different temperatures and time periods. b) twin fraction as a function of annealing temperature and time.

Twin boundary fraction is calculated using EBSD in samples annealed at 900-1100°C for different time periods. Similar conditions were maintained for all the samples and the corresponding grain boundary mapping images and the twin volume fractions are shown in Figures 4.10 (a) and 4.10(b) respectively. The blue colored lines represent the annealing twins corresponding 60° <111> family.

It is observed that with increasing the annealing time there is no considerable change in the twin fraction in samples annealed at 900 and 1000 and 1100°C. However, there is a sudden increase in the twin volume fraction with increasing the annealing temperature from 1000 to 1100°C. As mentioned above at 1100°C, dissolution of BCC/B2 precipitates which are rich in Al and Ni content, occurs. The dissolved Al and Ni solute atoms preferentially segregating to the stacking faults and lowering the stacking fault energy, Suzuki effect. This lowering stacking fault energy may be the reason for sudden increase in the twin volume fraction in case of 1100°C samples compared to 1000°C. When compared to samples annealed at 900°C and 1000°C, samples annealed at 1100°C shows rapid grain growth due to dissolution of the BCC/B2 precipitates. According to grain growth accident model, rapid grain boundary migration leads to formation of annealing twins due to stacking error. which may further increase the twin volume fraction at 1100°C.

4.2 Hardness measurement:

Hardness tests provide the preliminary data to measure the resistance of a material to permanent deformation. VHN is determined from the following equation.

$$VHN = 1.854 \, P \, / L^2$$

where p – is the load applied (kg)and, L – is the average diagonal lengths (mm)

The hardness was measured at a load of 0.3Kgf with dwell time of 15 secs and minimum 20 readings were taken for each sample.

Average Vickers hardness as a function of the grain size is shown Figure 4.11 (a) and 4.11(b), and indentation in made by diamond-pyramid indenter was shown in Figure 4.12. It is observed that, with increasing the annealing time the hardness of the material decreasing in samples

annealed at 900°C and 1000°C and it may be due to the increasing in grain size. The rate of decrease in hardness at a constant annealing time is more from 1000 to 1100°C compared to 900 to 1000°C. It may be due the fact that in later case only increasing grain size contributing the softening where at 1100°C both increasing grain size and dissolution of BCC phase may be contribution to the softening.
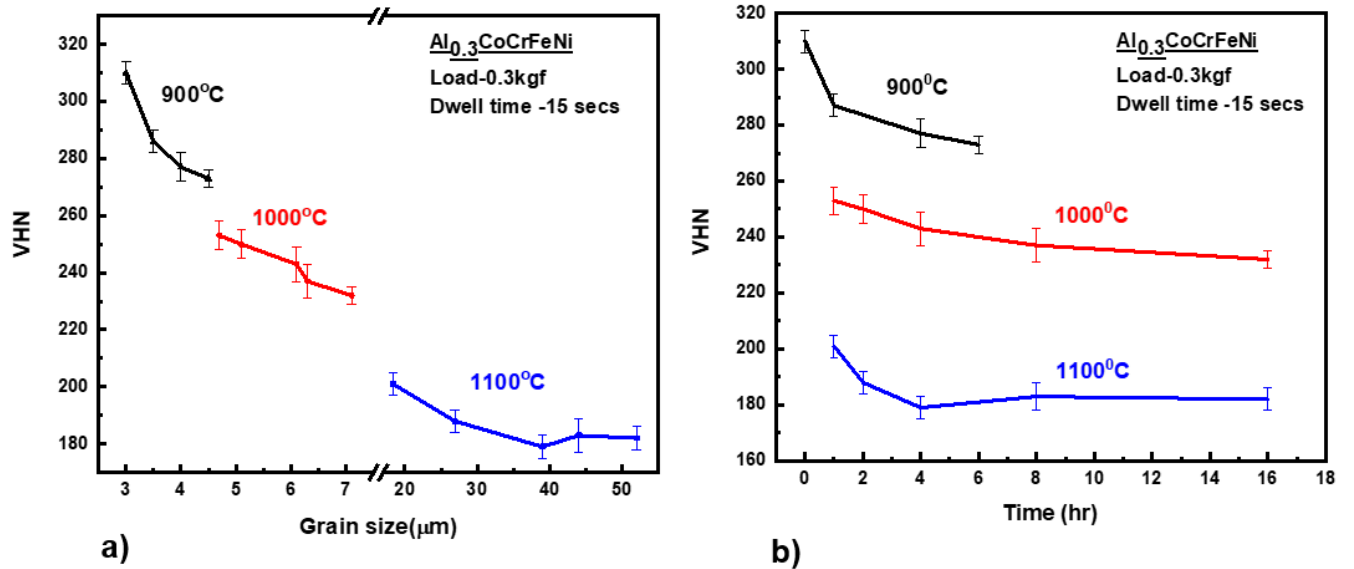
Figure 4.11 Hardness variation with(a) grain size and (b) annealing temperature and time.
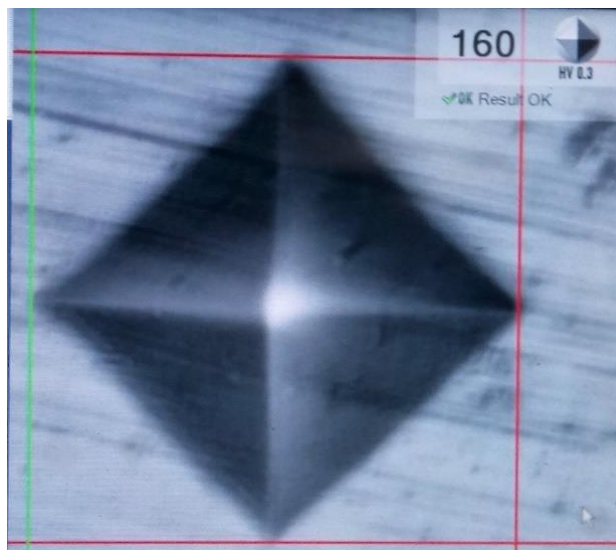
Figure 4.12 Indentation in made by diamond-pyramid indenter

4.5 Tensile test at room temperature:

Tensile testing was performed on dog boned shape specimen. The dimensions of the specimen were shown in Figure 4.13. The sample strains were calculated using digital image correlation (DIC). Speckle pattern created on the sample using spray gun is shown in Figure 4.14 for strain calculation. Vic Snap software was used to capture the images during the experiment, with an acquisition rate of 500 mill-seconds and the post processing of the captured images to calculate strain was done using VIC 2D software. VIC 2D uses the digital image correlation technique to provide strain measurements in a two-dimensional contour map as shown in figure 4.15. The image correlation done by using speckle pattern on the specimen, based on the displacement of the speckles from the reference image i.e. through incremental correlation of speckles from start to end of the test. During VIC 2D analysis subset size used is 33 and step size 7 and the 12mm^2 area was selected such that length of the box is equal to the gauge length of the specimen.
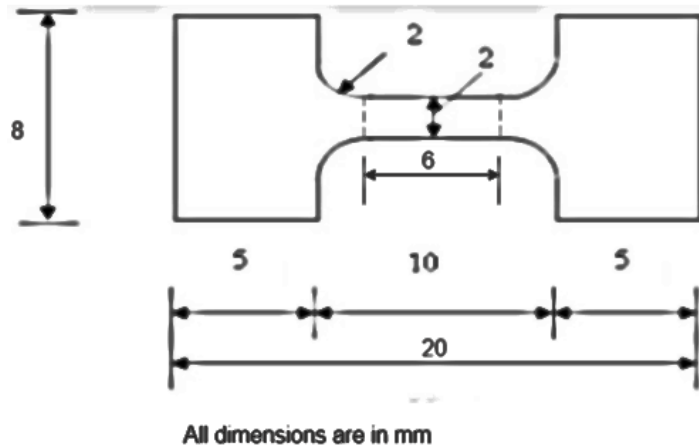
Figure 4.13 Schematic diagram of the dog bone shaped tensile specimen
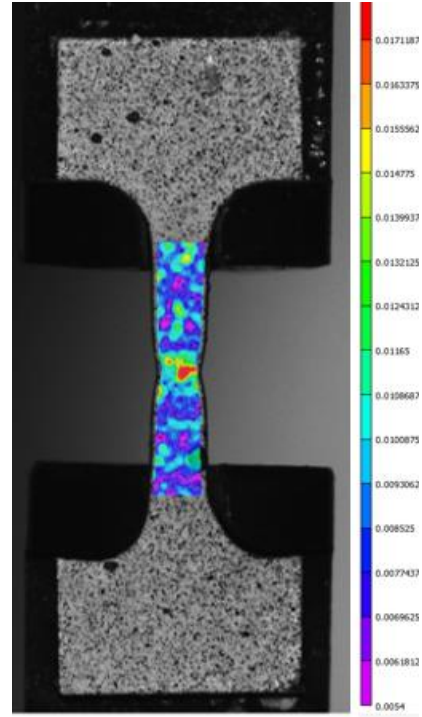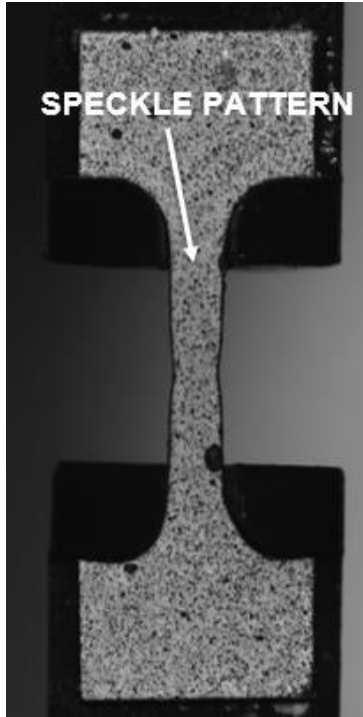
Fig4.14 Tensile specimen with speckle pattern   Fig 4.15 Strain variation along the gauge length

Room temperature tensile experiments were conducted for samples annealed at different time and temperatures having   different grain sizes at 10^{-3} s^{-1} strain rate and the corresponding engineering stress strain curves are showing in Figure 4.16.   The stress strain curve shows significant yield drop in all specimens. According to Johnston and Gilman theory yield drop in pure metals is due to lack of mobile dislocations in the specimen to maintain the constant applied strain rate.

The relation between the strain rate imposed and the dislocation density is given by the following equation.

$$\dot{\boldsymbol{\varepsilon}} = \mathsf{b\rho v} \ \ldots\ldots\ldots\ldots\ \mathsf{Eq(4)}$$

where ρ – is the density, b –is the burgers vector and v -is the average dislocation velocity

The dislocations density increases with deformation. Velocity (v) depends on the stress. In materials with limited mobile dislocations the imposed strain can be maintained by increment in the velocity(v) of dislocation. The velocity is strong function of stress so yield stress of the material

increases. But once the initial dislocations start moving they began to multiple and increases the dislocation and drop in yield stress occurs and further deformation increase the dislocation density and causes strain hardening.

In fine grain materials decreasing in grain size increase the grain boundary area. These grain boundaries act as dislocation sinks, and limits the dislocation density leads to yield drop in the specimen [40]. But in our case not only the specimens having fine grains annealed at 900°C and 1000°C and also specimens annealed at 1100°C with coarse grain size still showing yield drop (shown in insert). Some studies reported the presence of coherent precipitates causes the yield drop in material [24]. But no precipitates were observed in samples annealed at 1100°C. The understanding of the yield drop in our material need some more experiments which were not performed in the present thesis. Otto.*et.al.* [41] reported similar distinct yield point in fine grained CoCrFeNiMn alloy at temperatures of 25°C (293K) and 200°C (473K), but not at other temperatures and grain sizes. It is unclear whether this discontinuous yielding phenomenon is an intrinsic grain size effect or it might be due to the dislocation pinning and breaking away from solute atmospheres or short-range order.
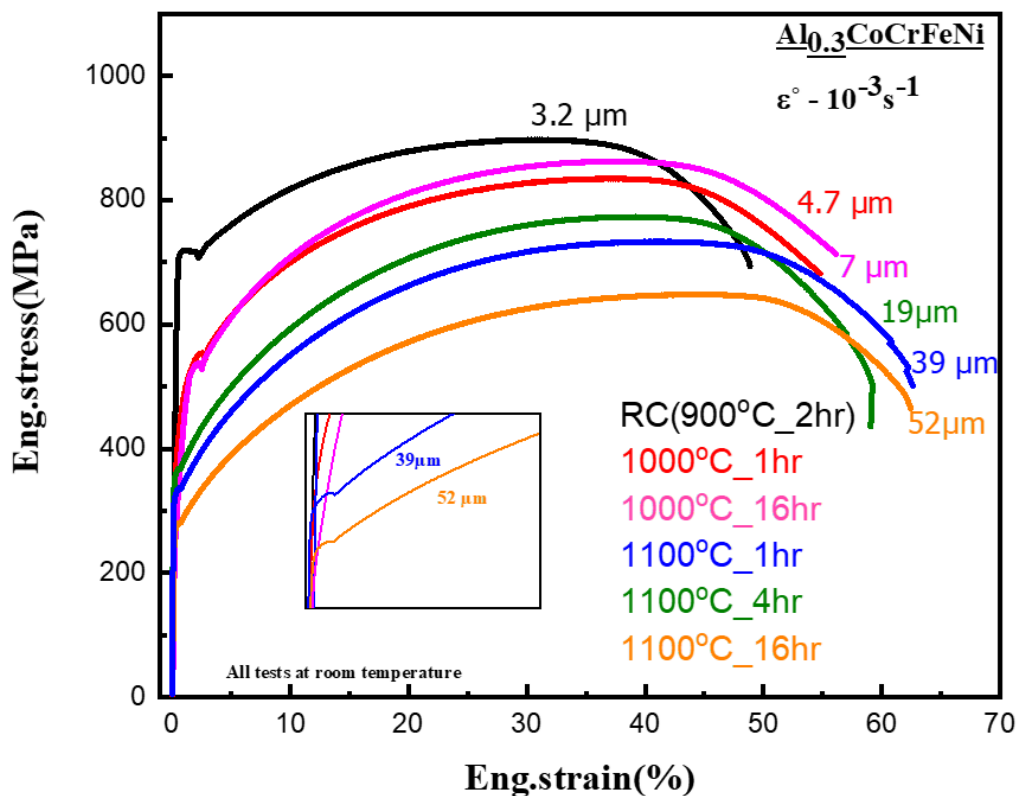
Figure 4.16 Engineering stress –strain curve of annealed specimens with different grain size.

Annealing condition	Phase	Grain size (μm)	Yield strength (MPa)	UTS (MPa)	Elongation (%)
900°C_2hr(RC)	FCC+B2	3.2±0.1	714	899	48
1000°C _1hr	FCC+B2	4.7±0.1	553	855	54
1000°C _16hr	FCC+B2	7±0.1	547	860	56
1100°C _1hr	FCC	19±1.0	368	773	59
1100°C _4hr	FCC	39±2.0	338	733	62
1100°C _16hr	FCC	52±2.0	281	648	69

Table4. Room temperature tensile properties of thermo-mechanically processed $Al_{0.3}CoCrFeNi$ HEA
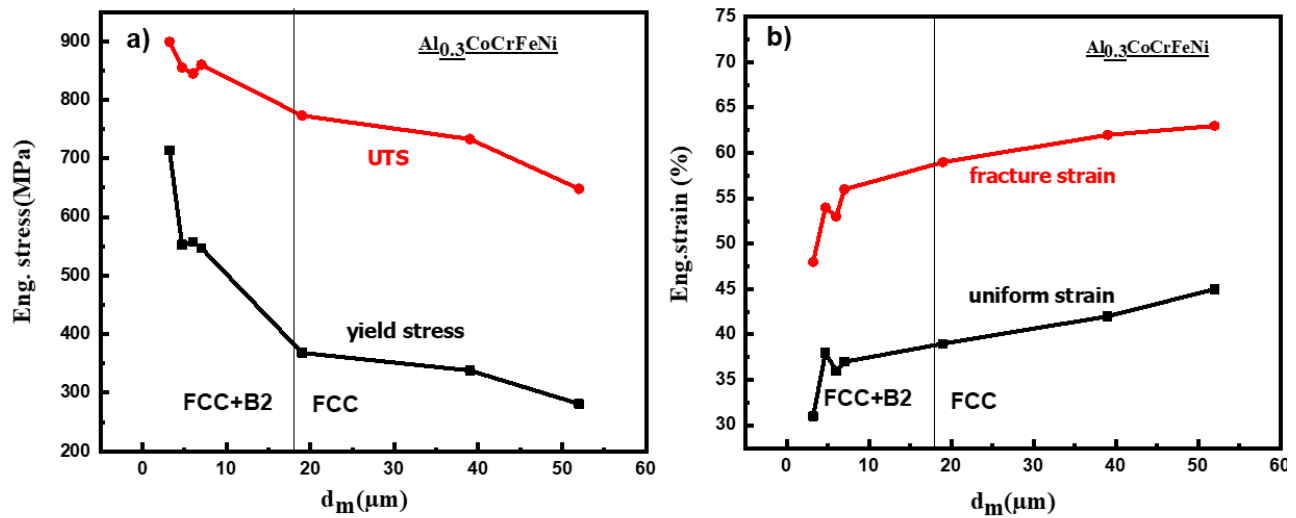
Figure 4.17 (a) variation of (a) yield stress and UTS and (b) uniform strain and fracture strain as a function of the grain size.

Yield strength, ultimate tensile strength along with ductility were calculated from stress-strain curves and plotted in figure 4.17 and the values are summarized in table 4. Annealed samples at temperatures 900ºC, 1000ºC, having FCC phase with B2 precipitates, shows higher yield strength more than 500 MPa. Especially, good combination of ultimate tensile strength (899MPa) and elongation (48%) was observed in recrystallized sample which is nearly equivalent to TRIP (UTS 600-900 MPa, elongation of 23-30%) and TWIP (UTS >800 MPa, elongation of >50%)steels [42] [43] [44]. Whereas samples annealed at 1100ºC with no B2 precipitates, displays low strength but higher ductility. which clearly indicates that the higher strength in 900ºC, 1000ºC annealed samples is due to fine grain size and presence of hard BCC/B2 precipitates.

4.6 Fractography:

Fracture surface of the deformed samples was observed using SEM. Fracture surface of the annealed at 900ºC for 4hr is shown in figure 4.18. Cup like appearances of the fracture surface was observed. Dimples and micro-voids on the fracture surface clearly indicates the ductile failure. Micro-voids shown in figure 4.18(a-b) may be the interface between parent FCC phase and BCC/B2 precipitates. The interface will act like a source of crack nucleation due to incompatibility in deformation.

Figure 4.18 Fractography images of annealed sample at 900°C for 4hr a) fracture tip b) fracture surface

4.5 Tensile tests at high temperature:

The microstructural studies of Al0.3CoCrFeNi HEA annealed at 900, and1000ºC, revealed the formation of fine B2(BCC) precipitates at grain boundaries. The presence of fine precipitates limited the grain growth of parent FCC phase by pinning the grain boundary, resulted very fine (<10 µm) and stable grains. Grain size measurements along rolling direction and along trans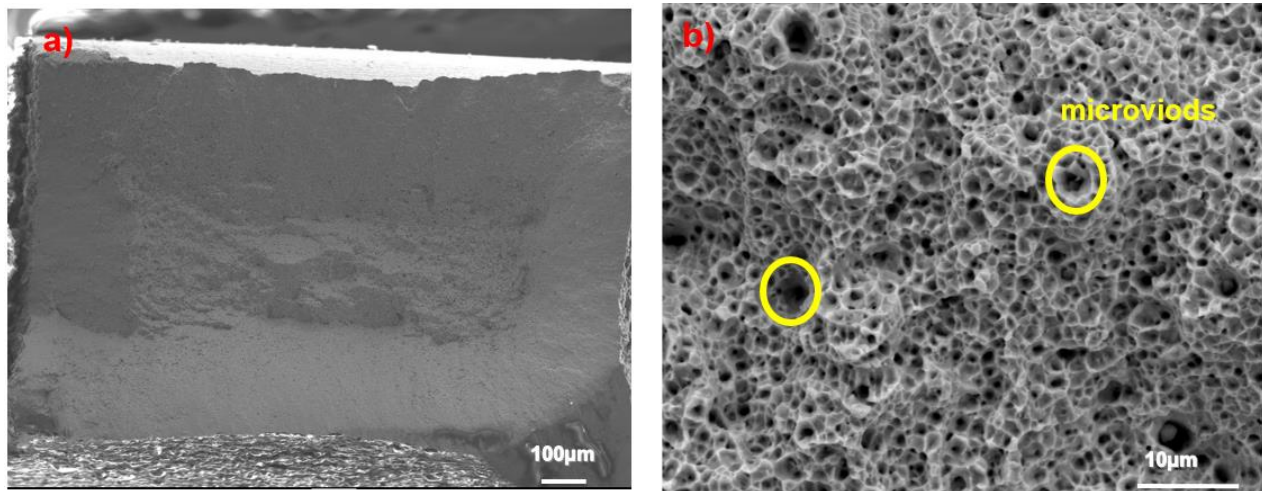verse direction reveals that grains are equiaxed. Fine, stable, equiaxed grains is the one of the microstructural prerequisite for superplasticity. Hence $Al_{0.3}CoCrFeNi$ alloy has very high tendency to exhibit superplastic behavior. To explore the possibility of superplasticity in $Al_{0.3}CoCrFeNi$, tensile experiments were performed on fine grain sized material as a function of temperature and strain rate.

$Al_{0.3}CoCrFeNi$ HEA annealed at temperatures 900ºC for 4hrs, with the average grain size of 3.5 um was chosen for high temperature tensile test and the corresponding microstructure is shown in figure.4.4(a). Tensile tests were conducted at temperatures 600,700, and 800ºC and at different strain rates ranging from $10^{-1}s^{-1}$ to $10^{-1}s^{-1}$. Figure 4.19 shows the tensile deformation behavior at different temperatures and different strain rates.

The tensile behavior at strain rate $10^{-3}s^{-1}$ shown in 4.19(b). During the tensile deformation at 200ºC, the material started yielding plastically at 680 MPa. The flow stress reached to maximum 846 MPa and then gradually decreased until it fails at 43% of elongation. Interestingly the material still shows yield point (shown in insert) even at 200ºC. The sample tested at 400ºC shows serrations on stress-strain curve, and also exhibit low ductility (∼ 36%) compared to the sample tested at 200ºC.Similar kind of deformation behavior was observed by Otto et al., [41] in fine grained CoCrFeMnNi alloy tested at 200 and 400ºC. It reported that this might be due to the presence of short range ordering(SRO) of solute atoms. The solute atoms increase in the yield stress by dislocation pinning, when stress is sufficiently high the motion of dislocation through ordered region randomizes the distribution of solute atoms and makes easy way for motion of subsequent dislocations results in yield drop. Still the reason for yield point phenomena is unclear so further investigation is needed to understand the possible reason.
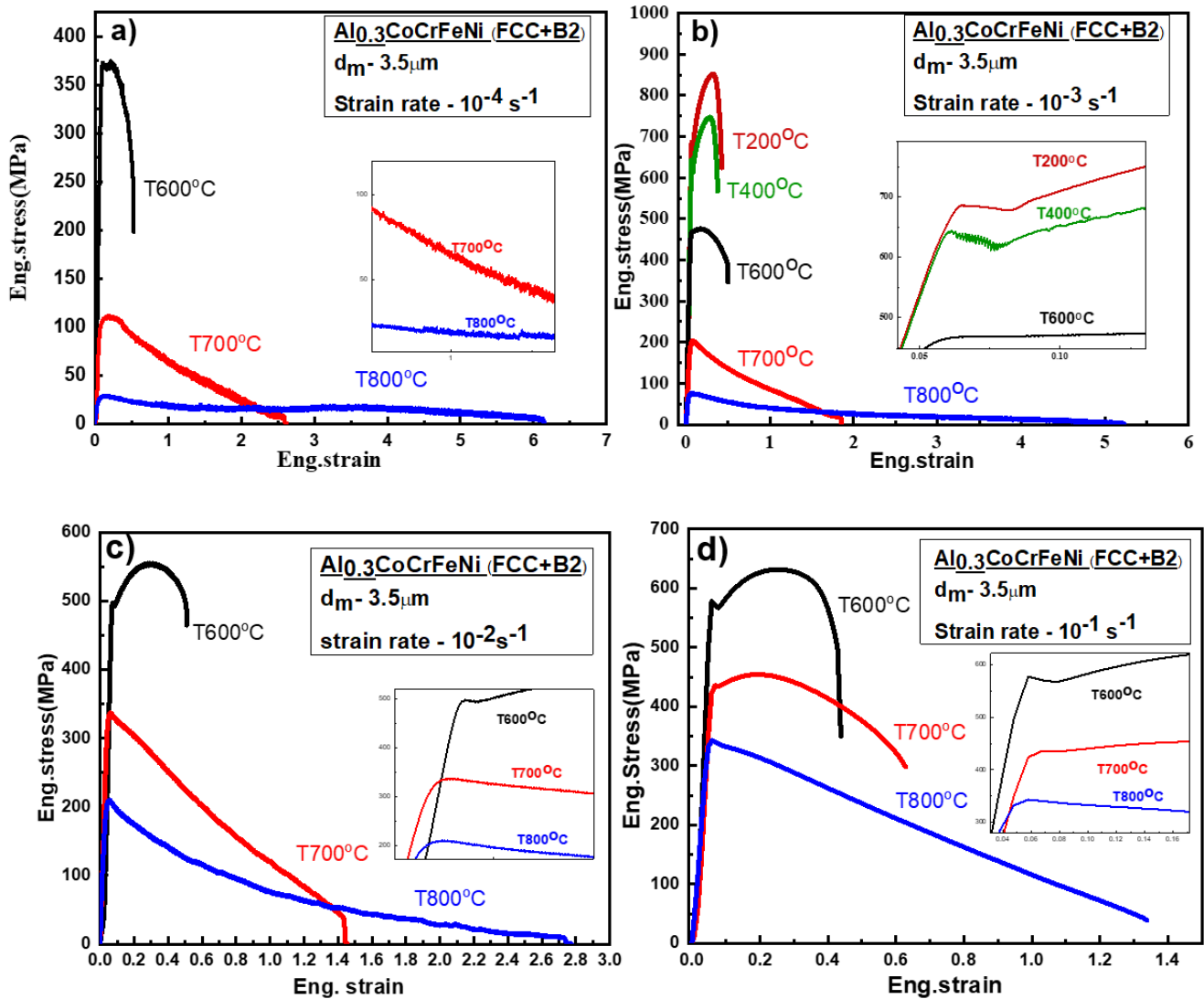
Figure 4.19 Eng. Stress–strain curves of $Al_{0.3}CoCrFeNi$ HEA tested strain rates a) $10^{-4}\,s^{-1}$ b) $10^{-3}\,s^{-1}$ c) $10^{-2}\,s^{-1}$ d) $10^{-1}\,s^{-1}$. At each strain rate stress-strain curves are shown for different temperatures.

The yield point phenomena appeared in all the samples tested at $600^{o}C$ at all strain rates. Further increasing the testing temperature and decreasing the strain rates promoting flow softening. Significant amount of strain hardening during initial stages of deformation was observed in the samples deformed at temperatures below $600^{o}C$ at all strain rates. During the initial at 700 and $800^{o}C$ (only at $10^{-2}s^{-1}, 10^{-1}s^{-1}$), the flow stress increased and then after reaching the peak value, softening occurred until it failed. Steady state flow was observed at $800^{o}C$ at $10^{-3}\,s^{-1}$ and $10^{-4}\,s^{-1}$. Maximum ductility of 614% is achieved at $800^{o}C$ testing temperature and at $10^{-4}\,s^{-1}$ strain rate and at different temperatures: $600,700,800^{o}C$ along with undeformed sample are shown in figure 4.20.
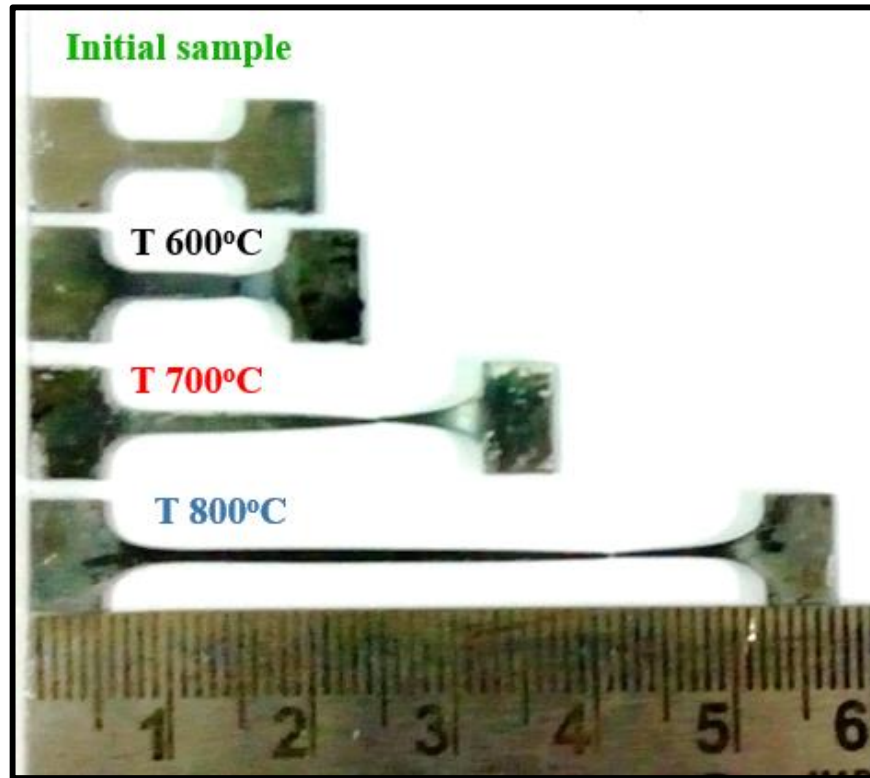
Figure 4.20 initial sample and deformed samples different temperatures at $10^{-4}s^{-1}$

The tensile properities of thermomechanically processed $Al_{0.3}CoCrFeNi$ tested at different temperatures and strain rates are summeriezed in table 5. The dependence of tensile properities on temperature and strain rate are plotted in figaure 4.21 suggesting that increasing the testing temperature and decreaing strian rate decreasing both the yield strength(σ_0),and ultimate tensile strength (UTS),and increasing the elongation to failure. For example, sample tested at $600^{O}C$ shows decrease in yield stress and UTS , respectivly from 530 MPa to 296 MPa and 625 MPa to 373 MPa . But there is no significant change in the elongation. Flow softening at $700^{o}C$ increases the elongation upto 260% with decreasing the strain rate and the increment in elogation accompained by decreasing the yield stength from 422 to 69 MPa and UTS from 453 to 111 MPa.The maximum elongation of 614% was observed at $800^{o}C$ temperature and $10^{-4}s^{-1}$ strain rate.

41

Temperature	200°C	400°C	600°C				700°C				800°C			
Strain rate (s^{-1})	10^{-3}	10^{-3}	10^{-1}	10^{-2}	10^{-3}	10^{-4}	10^{-1}	10^{-2}	10^{-3}	10^{-4}	10^{-1}	10^{-2}	10^{-3}	10^{-4}
Yield stress(MPa)	680	640	530	483	395	296	422	378	165	69	292	153	48.5	18.5
UTS (MPa)	846	747	625	585	475	373	453	420	203	111	332	209	75	30
Elongation(%)	43	37.6	44	50	50	52	62	87	185	260	133	273	521	614

Table 5 High temperature tensile properites at different strian rates
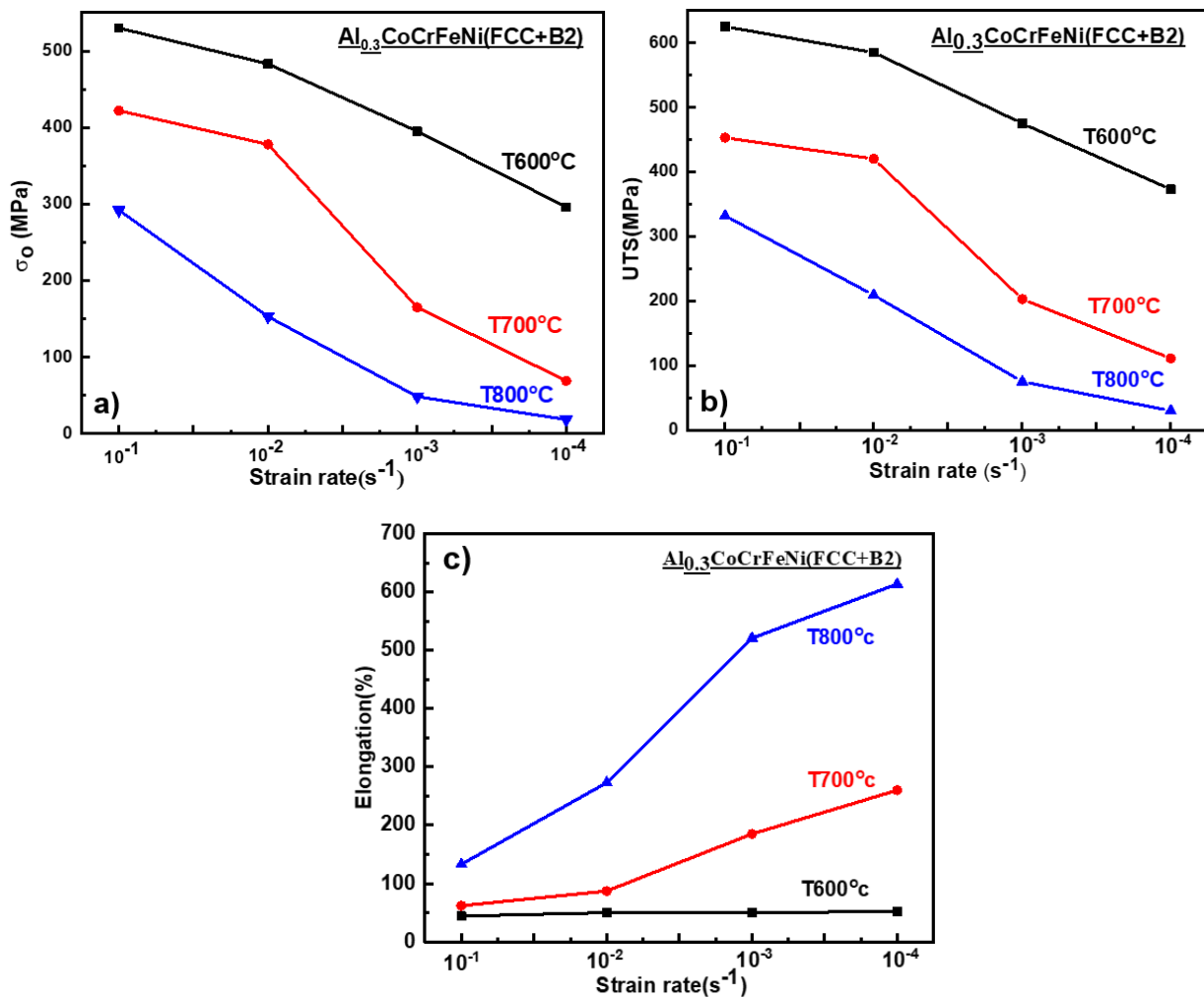
Figure 4.21 Effect of temperature and strain rate on a) yield stress and b) UTS c) Failure elongation

The effect of temperature on strain rate sensitivity (m) was plotted in figure 4.22. The strain rate sensitivity (m) values were measured to be 0.08, 0.27, 0.41 for temperatures 600, 700, and 800°C, respectively shows that strain rate sensitivity is strongly temperature dependent. The measured m value for 800°C is 0.4 indicating that Grain boundary sliding(GBS) may be the dominant mechanism responsible for superplastic elongation. However, the conformation of the deformation mechanism needs post deformation microstructural.
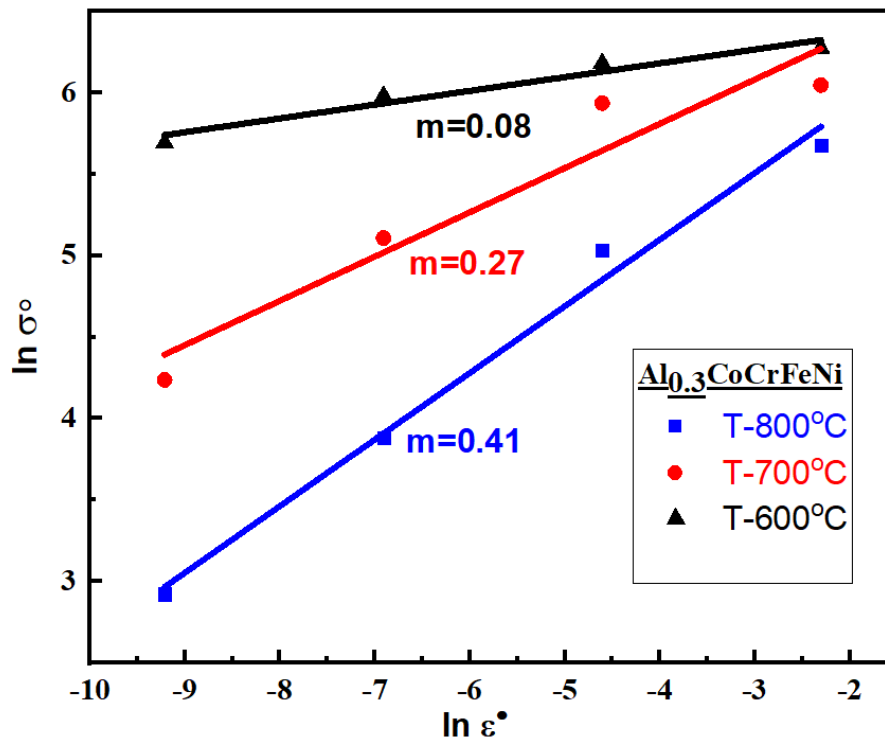
Figure 4.22 Flow stress corresponds to 0.002 strain plotted as a function of strain rate for $Al_{0.3}CoCrFeNi$ HEA tested at 600, 700, and 800°C.

Fractography:

The SEM images of fracture surface samples deformed at 600, 700, and 800°C at $10^{-4}s^{-1}$ strain rate are shown in figure 4.23. and clearly showing the dimple like fracture which is a clear indication of ductile fracture.
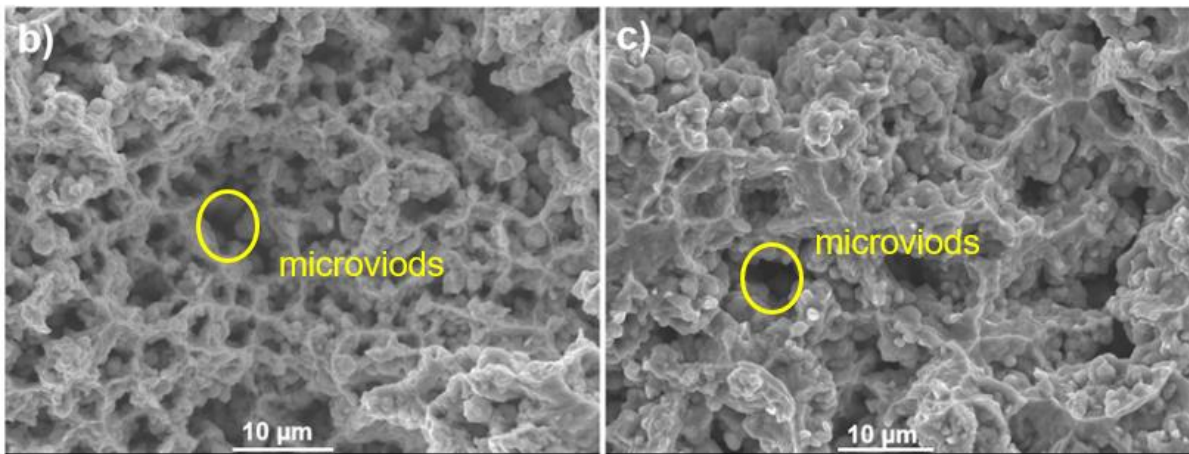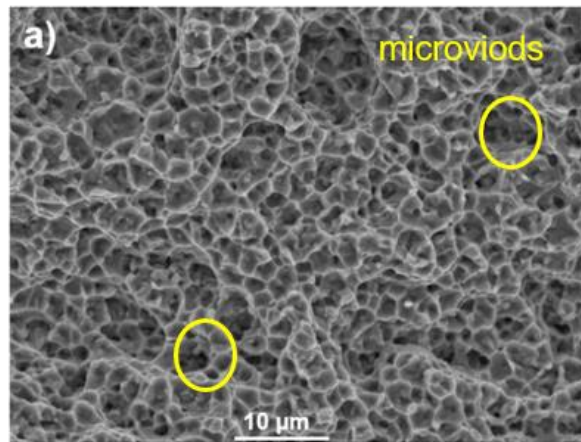
Figure 4.23. The SEM images of fracture surface samples deformed at a) 600°C, b) 700°C c) 800°C at strain rate $10^{-4}s^{-1}$.

Chapter 5: Summary and Conclusions

In this study we investigated the effect of temperature and strain rate on flow behavior of $Al_{0.3}$CoCrFeNi HEA. Initially studies focused on the microstructure evolution and phase stability of cold rolled Al0.3CoCrFeNi HEA annealed at different temperatures and time periods. The microstructural analysis revealed the fine, stable grain structure with B2(BCC) precipitates along FCC parent phase grain boundaries and triple points. Grain size measurement was done in RD and TD directions and concluded that grains are equiaxed. Annealing twins were also formed in the material.

To understand the flow behavior tensile experiments were performed at room temperature and observed that annealed samples at temperatures 900ºC, 1000ºC, having FCC phase with B2 (BCC)precipitates, shows higher yield strength, more than 500 MPa. Good combination of ultimate tensile strength (899MPa) and elongation (48%) was observed in samples recrystallized at 900ºC for 2hr. Whereas Samples annealed at 1100ºC with no B2 precipitates, exhibit low strength but higher ductility, clearly indicating that fine grain size and presence of hard B2(BCC) precipitates are the reasons for the higher strength in 900 and, 1000ºC annealed samples.

Tensile samples with fine equiaxed grains with a grain size of 3.5 μm tested at different temperature (200ºC to 800ºC) and strain rates (10^{-1} to 10^{-4} s^{-1}) and observed superplastic behavior at 800ºC temperature and 10^{-4} and $10^{-3}s^{-1}$ strain rate. Elongation to failure of 520% at 800ºC, $10^{-3}s^{-1}$ and 614% at $10^{-4}s^{-1}$ strain rates are observed. The yield strength and UTS decreasing with increasing temperature and decreasing strain rate. The strain rate sensitivity m=0.41 was obtained at 800ºC suggesting grain boundary sliding may be responsible mechanism for the observed superplastic behavior.

Fracture surface of the deformed samples were studied using SEM and observed dimple fracture which represents the typical ductile fracture.

Future Work

The effect of temperature and strain on flow behavior was investigated in this work. Certain problems needed to be investigated further to understand underlying deformation behaviors mechanism.

- The possibility of superplasticity at 900ºC at different strain rates need to be explored.
- The mechanism responsible for superplastic flow behavior is need to be investigated from post deformation microstructure analysis.
- The causes for sudden yield drop during room temperature tensile tests is need to investigated.

References

[1] B. Cantor, I. T. H. Chang, P. Knight, and A. J. B. Vincent, "Microstructural development in equiatomic multicomponent alloys," *Mater. Sci. Eng. A*, vol. 375–377, no. 1–2 SPEC. ISS., pp. 213–218, 2004.

[2] J. W. Yeh *et al.*, "Nanostructured high-entropy alloys with multiple principal elements: Novel alloy design concepts and outcomes," *Adv. Eng. Mater.*, vol. 6, no. 5, p. 299–303+274, 2004.

[3] D. Miracle, O. Senkov, Acta Mater. 122 (2017) 448–511.

[4] Z.S. Nong, D.S. Li, J.C. Zhu, H.L. Yu, Z.H. Lai, Effect of aluminum content on microstructure and wear resistance of CuCrFeMnTiAlx high-entropy alloy, Rare Metal. Mat. Eng. 40 (2011) 550e554

[5] Y.-L. Chou, Y.-C. Wang, J.-W. Yeh, H.-C. Shih, Pitting corrosion of the highentropy alloy Co1.5CrFeNi1.5Ti0.5Mo0.1 in chloride-containing sulphate solutions, Corros. Sci. 52 (2010) 3481e3491.

[6] Y.-L. Chou, J.-W. Yeh, H.-C. Shih, The effect of molybdenum on the corrosion behavior of the high-entropy alloys Co1.5CrFeNi1.5Ti0.5Mox in aqueous environments, Corros. Sci. 52 (2010) 2571e2581

[7] Z.J. Wang, S. Guo, Q. Wang, Z.Y. Liu, J.C. Wang, Y. Yang, C.T. Liu, Nanoindentation characterized initial creep behavior of a high-entropy-based alloy CoFeNi, Intermetallics 53 (2014) 183e186.

[8] L.J. Zhang, P.F. Yu, H. Cheng, H. Zhang, H.Y. Diao, Y.Z. Shi, B.L. Chen, P.Y. Chen, R. Feng, J. Bai, Q. Jing, M.Z. Ma, P.K. Liaw, G. Li, R.P. Liu, Nanoindentation creep behavior of an Al0.3CoCrFeNi high-entropy alloy, Metall. Mater. Trans. A 47 (12) (2016) 5871e5875.

[9] M.A. Hemphill, T. Yuan, A.M. Wang, J.-W. Yeh, C.-W. Tsai, A. Chuang, P.K. Liaw, Fatigue behavior of Al0.5CoCrCuFeNi high entropy alloys, Acta Mater 60 (2012) 5723e5734.

[10] H.-P. Chou, Y.-S. Chang, S.-K. Chen, J.-W. Yeh, Microstructure, thermophysical and electrical properties in AlxCoCrFeNi (0_x_2) high-entropy alloys, Mater. Sci. Eng. B 163 (2009) 184e189.

[11] C.-L. Lu, S.-Y. Lu, J.-W. Yeh, W.-K. Hsu, Thermal expansion and enhanced heat transfer in high-entropy alloys, J. Appl. Crystallogr. 46 (2013) 736e739.

[12] D. Zhang, Deformation twinning (update), Ref. Modul. Mater. Sci. Mater. Eng.(2016), https://doi.org/10.1016/B978-0-12-803581-8.02878-2.

[13] C.-W. Tsai, Y.-L. Chen, M.-H. Tsai, J.-W. Yeh, T.-T. Shun, S.-K. Chen, Deformation and annealing behaviors of high-entropy alloy Al0.5CoCrCuFeNi, J. Alloys Compd. 486 (2009) 427e435.

[14] M.-H. Tsai and J.-W. Yeh, "High-Entropy Alloys: A Critical Review," Mater. Res. Lett., vol. 2, no. 3, pp. 107–123, 2014.

[15] B. S. Murty, J. W. Yeh, and S. Ranganathan, "High Entropy Alloys," *High Entropy Alloy.*, no. January, pp. 159–169, 2014.

[16] J. W. Yeh, "Physical Metallurgy of High-Entropy Alloys," *Jom*, vol. 67, no. 10, pp. 2254–2261, 2015.

[17] W.-R. Wang, W.-L. Wang, S.-C. Wang, Y.-C. Tsai, C.-H. Lai, and J.-W. Yeh, "Effects of Al addition on the microstructure and mechanical property of AlxCoCrFeNi high-entropy alloys," *Intermetallics*, vol. 26, pp. 44–51, 2012.

[18] K. Y. Tsai, M. H. Tsai, and J. W. Yeh, "Sluggish diffusion in Co-Cr-Fe-MnNi high-entropy alloys," *Acta Mater.*, vol. 61, no. 13, pp. 4887–4897, 2013.

[19] S. Praveen, J. Basu, S. Kashyap, and R. S. Kottada, "Exceptional resistance to grain growth in nanocrystalline CoCrFeNi high entropy alloy at high homologous temperatures," *J. Alloys Compd.*, vol. 662, pp. 361–367, 2016.

[20] B. R. Chen, A. C. Yeh, and J. W. Yeh, "Effect of one-step recrystallization on the grain boundary evolution of CoCrFeMnNi high entropy alloy and its subsystems," *Sci. Rep.*, vol. 6, no. February, pp. 1–9, 2016.

[21] W. H. Liu, Y. Wu, J. Y. He, T. G. Nieh, and Z. P. Lu, "Grain growth and the Hall-Petch relationship in a high-entropy FeCrNiCoMn alloy," *Scr. Mater.*, vol. 68, no. 7, pp. 526– 529, 2013

[22] S. Ranganathan, "Alloyed pleasures: Multimetallic cocktails," *Curr. Sci.*, vol. 85, no. 10, pp. 1404–1406, 2003.

[23] W.-R. Wang, W.-L. Wang, S.-C. Wang, Y.-C. Tsai, C.-H. Lai, and J.-W. Yeh, "Effects of Al addition on the microstructure and mechanical property of AlxCoCrFeNi high-entropy alloys," *Intermetallics*, vol. 26, pp. 44–51, 2012.

[24] T. T. Shun and Y. C. Du, "Microstructure and tensile behaviors of FCC Al0.3CoCrFeNi high entropy alloy," *J. Alloys Compd.*, vol. 479, no. 1–2, pp. 157–160, 2009

[25]Qiao, J.W., S.G. Ma, E.W. Huang, C.P. Chuang, P.K. Liaw, and Y. Zhang, *Microstructural characteristics and mechanical behaviors of AlCoCrFeNi highentropy alloys at ambient and cryogenic temperatures.* Materials Science Forum, 2011. **688**: pp. 419-425.

[26]. M.O. Laktionova, E.D.T., Z. Tang, P.K. Liaw, *Low Temperature Mechanical Behavior of the Al0.5CoCrCuFeNi High-Entropy Alloy*, in *Materials Science andTechnology*. 2012: Pittsburgh, Pennsylvania, USA.

[27] S.G. Ma , S.F. Zhang J.W. Qiao , Z.H. Wang , M.C. Gao , Z.M. Jiao , H.J. Yang Y. Zhang Superior high tensile elongation of a single-crystal CoCrFeNiAl0.3 high-entropy alloy by Bridgman solidification

[28] Dongyue Li, Chengxin Li, Tao Feng, Yidong Zhang , Gang Sha ,John J. Lewandowski , Peter K. Liaw , Yong Zhang , High-entropy Al0.3CoCrFeNi alloy fibers with high tensile strength and ductility at ambient and cryogenic temperatures

[29] Nieh TG, Wadsworth J (1998) Fine-structure superplasticity in materials. J Chin Inst Eng 21:659–689

[30] Hashimoto, S., F. Moriwaki, T. Mimaki, and S.Miura, "Sliding Along the Interphase Boundary in Austenitic/Ferritic Duplex Stainless Steel Bicrystals," in *International Conference on Superplasticity in Advanced Materials (ICSAM-91),* edited by S. Hori, M. Tokizane, and N. Furushiro,The Japan Society for Research on Superplasticity,Osaka, Japan, pp. 23-32 (1991).

[31] Gifkins, R.C., "Grain Boundary Sliding and its Accommodation during Creep and Superplasticity,"*Metall. Trans.,* Vol. 7A, pp. 1225-1232(1976).

[32] Humphries, C.W. and N. Ridley, "Effect of Relatively Hard Particles on Cavitation of Microduplex Pb-Sn Eutectic During Superplastic Flow," *J. Mater. Sci.,* Vol. 12, pp. 851-855

[33].A.V. Kuznetsov, D.G. Shaysultanov, N.D. Stepanov, G.A. Salishchev, O.N. Senkov,Superplasticity of AlCoCrCuFeNi high entropy alloy, Mater. Sci. Forum 735 (2013) 146-151.

[34].H. Shahmir, J. He, Z. Lu, M. Kawasaki, T.G. Langdon, Evidence for superplasticity in a CoCrFeNiMn high-entropy alloy processed by high-pressure torsion, Mater. Sci. Eng. A 685(2017) 342-348

[35]H. Shahmir, M. Nili-Ahmadabadi, A. Shafiee, T.G. Langdon, Effect of a minor titanium addition on the superplastic properties of a CoCrFeNiMn high-entropy alloy processed by high-pressure torsion, Mater. Sci. Eng. A (2018) in press. DOI: 10.1016/j.msea.2018.02.002.

[36] S.R. Reddy, S. Bapari, P.P. Bhattacharjee, A.H. Chokshi, Superplastic-like flow in a fine-grained equiatomic CoCrFeMnNi high-entropy alloy, Mater. Res. Lett. 5 (2017) 408-414.

[37] W.R.Wang,W.L.Wang, S.C.Wang, Y.C. Tsai, C.H. Lai, J.W. Yeh, Effects of Al addition on the microstructure and mechanical property of AlxCoCrFeNi high-entropy alloys,Intermetallics 26 (2012) 44–51.

[38] Gwalani B, Soni V, ChoudhuriD, et al. Stability of ordered L1 2 and B 2 precipitates in face centered cubic based high entropy alloys-Al0.3CoFeCrNi and Al0.3CuFeCrNi2.Scripta Mater. 2016;123:130–134.

[39] Gwalani B, Choudhuri D, Soni V, et al. Cu assisted stabilization and nucleation of L1 2 precipitates inAl0.3CuFeCrNi2 fcc-based high entropy alloy. ActaMater.2017;129:170–182.

[40]Kamikawa, Naoya & Huang, Xiaoxu & Tsuji, Nobuhiro & Hansen, Niels. (2009). Strengthening mechanisms in nanostructured high-purity aluminium deformed to high strain and annealed. Acta Materialia. 57. 10.1016/j.actamat.2009.05.017.

[41] F. Otto, A. Dlouhý, C. Somsen, H. Bei, G. Eggeler, and E. P. George, "The influences of temperature and microstructure on the tensile properties of a CoCrFeMnNi high-entropy alloy," *Acta Mater.*, vol. 61, no. 15, pp. 5743–5755, 2013.

[42] Zhang, Yinghui & Ma, Yonli & Kang, Yonglin & Yu, Hao. (2006). Mechanical properties and microstructure of TRIP steels produced using TSCR process. Journal of University of Science and Technology Beijing, Mineral, Metallurgy, Material. 13. 416-419. 10.1016/S1005-8850(06)60084.

[43] Xiong, Zhi-ping & Kostryzhev, Andrii & Saleh, Ahmed & Chen, Liang & Pereloma, E. (2016). Microstructures and mechanical properties of TRIP steel produced by strip casting simulated in the laboratory. Materials Science and Engineering A. 664. 26–42. 10.1016/j.msea.2016.03.106.

[44] Kusakin, Pavel & Kaibyshev, Rustam. (2016). High-Mn twinning-induced plasticity steels: Microstructure and mechanical properties. 44. 326-360.